Experimental Evaluation of Laminated Glass Interlayer Polymers at Various Strain Rates and Temperatures

A Thesis Presented to the Faculty of the Graduate School of the

University of Missouri – Columbia

In Partial Fulfillment of the Requirements for the Degree

Master of Science In

Civil and Environmental Engineering

By

Jonathan Taylor Knight

Dr. Hani Salim, Thesis Supervisor

DECEMBER 2020

The undersigned, appointed by the dean of the Graduate School, have examined the thesis entitled

"Experimental Evaluation of Laminated Glass Interlayer Polymers at Various Strain Rates and Temperatures"

presented by Jonathan Taylor Knight,

a candidate for the degree of Master of Science in Civil and Environmental Engineering, and hereby certify that, in their opinion, it is worthy of acceptance.

Professor Hani Salim

Professor John Bowders

Professor John Gahl

Professor Alaaeldin Elsisi

DEDICATION

I dedicate my thesis work to my loving and supportive mother. Throughout my life, she has been the best parent, teacher, teammate, mentor, and friend that I could ever hope to be. Everything that I am and will be, I owe to her.

ACKNOWLEDGEMENTS

I would like to express my deepest appreciation for my committee chair, Professor Hani Salim, for his invaluable advice and spirited encouragement during the writing of this thesis.

I would like to thank my committee members Dr. John Bowders and Dr. John Gahl for their engaging questions and feedback, and Dr. Alaaeldin Elsisi for his assistance with the experimental setup and guidance in data analysis. Dr. Elsis's development of the photo-tracking software used in this research was instrumental.

I would like to thank Mr. Richard Oberto for his sage technical assistance, especially with calibration of the experimental program and implementation of the optical trigger.

I would also like to thank my fellow members of the research team, Dr. Aaron Saucier and Mr. Caleb Phillipps, for their mentorship and camaraderie, and fellow graduate student Brooke Dean for her help with the quasi-static testing.

Finally, I would like to offer my sincere appreciation for the financial support provided by Battelle Memorial Institute and valued collaboration with the Air Force Civil Engineer Center (AFCEC) at Tyndall Air Force Base and the United States Department of State.

TABLE OF CONTENTS

CONTENTS

LIST OF FIGURES

LIST OF TABLES

Experimental Evaluation of Laminated Glass Interlayer Polymers at Various Strain Rates and Temperatures

Jon Knight

Dr. Hani Salim, Thesis Supervisor

ABSTRACT

The use of blast-resistant glazing, such as laminated glass in buildings can greatly reduce, if not eliminate, the hazard of flying glass shards. In a failure event, fractured glass shards adhere to the polymer interlayer, and do not fly or fall. Under dynamic loading scenarios such as blast, the interlayer deforms largely, providing post-cracking energy absorption to the laminated glass system. When properly designed, laminated glass polymer interlayers are capable of maintaining the integrity of the building envelope in extreme events such as blasts or hurricanes, protecting the interior from damage. Analytical and experimental research exists in the literature in the area of blast-resistant glazing; however, more research on the dynamic response of polymer interlayer materials is necessary to understand the post-cracking behavior of blast-resistant window systems. Therefore, the main objective of this research is to experimentally evaluate the high strain rate and temperature effects on the dynamic response of pre-laminated PVB and SG polymers. The results of this research are expected to enhance the engineering design methods and

numerical modeling of laminated glass windows subjected to dynamic loading. A drop weight testing apparatus was used in this research for evaluating PVB and SG samples under various loading rates and at different temperature ranges. Quasi-static testing of the materials was performed using a servo hydraulic testing machine in order to evaluate the effects of dynamic loading on the engineering stress-strain response and energy absorption capabilities of the interlayer materials. The results show that dynamic loading significantly affects the engineering stress-strain response and energy absorption of the materials. Under quasi-static loading, PVB behaves in a highly non-linear, hyperelastic manner; however, the dynamic response of PVB is bilinear and viscoelastic. Dynamic loading of SG increases the initial modulus of the response by about 20% and pseudo-yield strength by about 60%, resulting in far greater energy absorption than the quasi-static response at the same strains. The effect of strain rate variation effects the initial linear region of the response of PVB more than the response after pseudo-yielding. In general, as strain rate increases, the initial modulus and pseudo-yield strength increase, resulting in increased total strain energy. Temperature effects are more prominent than the effect of strain rate variation on the dynamic response of PVB. At colder temperatures, the initial linear elastic response is predominant, and at elevated temperatures, the secondary viscoelastic response is predominant. The results of this thesis provide valuable findings regarding the dynamic response of interlayer polymers, but additional tests are still needed to develop statically reliable results. A wider range of strain rates is recommended to better understand the strain rate effects on the dynamic response of interlayer materials. More precise temperature control, and elimination of initial strains due to prestressing, are necessary to accurately characterize the temperature effects on the dynamic response of interlayer materials.

CHAPTER 1 - INTRODUCTION

1.1 BACKGROUND

In design of structures, occupant safety is the highest priority. External loads such as wind, snow, and loads from extreme events must be considered to ensure structural integrity and occupant safety. During extreme events such as hurricanes or blasts, the exterior envelope is the most vulnerable component of a structure because it is the front line of defense. The increase in terrorist attacks on densely populated urban areas in recent years has raised concerns about building safety and placed heightened importance on the design of building façades.

The exterior envelope of a building consists of wall systems, which contain windows and doors, and a roof system. For centuries, glass has been used for windows and façades because of its transparency and aesthetic appeal. Due to the relatively low tensile strength and brittle behavior of glass, compared to other structural materials such as concrete and steel, glass elements are typically fragile and are therefore the most vulnerable components of a building envelope to extreme loads such as air blast waves or impact from flying debris. And because of the brittleness and fragility of glass, failure of a glass pane subjected to an extreme load such as a blast wave sends fractured glass shards flying at high velocities, which can lead to enormous causalities. As a result, it is vitally important to human safety to properly understand the actual behavior of structural glass elements under extreme loads.

In a blast event, air blast waves can cause glass windows to shatter hundreds of meters from the detonation source. For instance, the 1995 Oklahoma City bombing attack broke windows and shattered fragments about 1000 meters away from the explosion source (Zhang & Bedon, 2017). Glass-related injuries due to blast events can account for a significant proportion of total injuries. In the case of the Oklahoma City bombing attack, researchers reported that 39% (200 out of 508) of injured persons suffered glass-related injuries (Norville et al., 1999). At the same time, air blast pressure entering buildings can cause extensive hearing damage. Of the injured survivors of the Oklahoma City bombing attack, 265 indicated they suffered some degree of hearing impairment, and of these, 230 (87%) were located inside buildings (Norville et al., 1999). Therefore, the use of blast-resistant glazing, such as laminated glass, can significantly reduce hearing and flying glass injuries. (Norville et al., 1999)

Laminated glass (LG) is the most widely used glazing material for safety. Laminated glass consists of two or more layers of glass with a polymer interlayer such as polyvinyl butyral (PVB) or SentryGlas® (SG) between the glass layers. In a failure event, the fractured glass particles adhere to the polymer interlayer and do not fly or fall. Additionally, after glass cracking, the ductile polymer interlayer deforms significantly as a continuous membrane. In a blast event, the polymer interlayer may provide enough post-breakage energy absorption for the fenestration to remain intact, preventing the air blast wave from entering into the building. Therefore, laminated glass is an excellent glazing material for safety because it greatly reduces glass-related injuries by retaining a majority of the glass shards after failure and, if designed properly, mitigates hearing-related injuries associated with blast events by preventing the air blast wave from

entering the building (Norville et al., 1999). However, the behavior of laminated glass under dynamic loading is extremely difficult to properly characterize because it depends on the mechanical behavior of the polymer interlayer, which is typically strain-rate and temperature dependent (Martín et al., 2020). More research on the strain-rate and temperature dependent mechanical properties of polymer interlayers is necessary to better understand the dynamic response of laminated glass. Therefore, in this research, the dynamic response of interlayer materials PVB and SG will be experimentally evaluated at various strain rates and temperature ranges.

1.2 OBJECTIVES

The goal of this research is to experimentally evaluate the high strain rate and temperature effects on the dynamic response of pre-laminated PVB and SG polymers. The results of this research are expected to enhance the mechanical characterizations of these materials and, consequently, the analytical and numerical modeling of the dynamic response of laminated glass systems.

To achieve the objective of this project, the following tasks are realized:

- Collect and summarize relevant literature in area of mechanical evaluation of laminated glass systems and interlayer polymers.
- Validate and advance the existing drop-weight testing methodology for evaluating polymer interlayers under various loading rates.

- Experimentally evaluate PVB and SG under high strain rates and quasi-static loading.

  Experimentally evaluate the high strain rate behavior of PVB at various temperatures and loading rates.

1.3 SCOPE AND ORGANIZATION

This study focusses primarily on mechanical properties of laminated glass interlayer polymers in relation to the blast resistance of structural laminated glass; however, the implications of this study can be applied to the study of laminated glass for a wide range of uses such as storm resistance, burglar resistance, automotive applications, etc.

The organization of this thesis is as follows:

- Chapter 1 contains an introduction, the objectives, and the scope and organization of the research.
- Chapter 2 presents an extensive literature review detailing the problem statement and need for research, the materials studied in this research, and the methodologies used to achieve the objectives of this research.
- Chapter 3 describes the experimental designs, testing apparatuses, and test setups.
- Chapter 4 presents an analysis and discussion of the experimental results.
- Chapter 5 states the main conclusions, proposes recommendations, and discuss future research continuing the research presented in this thesis

CHAPTER 2 - LITERATURE REVIEW

2.1 INTRODUCTION

This chapter details the problem statement and need for more research, general information and results of previous studies about the materials investigated in this research, namely laminated glass, polyvinyl butyral (PVB), and SentryGlas® (SG), and the general experimental procedures of high strain rate, quasi-static, and drop weight testing utilized in this research to achieve the objective.

The increase in worldwide terrorist attacks on civilians since the 1970's has placed a heightened significance on the blast resistance of structures, and specifically windows and façades as they are at the front line of defense and most vulnerable components of the exterior envelope of a structure. According to the Global Terrorism Database (University of Maryland, 2020) the average worldwide deaths per year from terrorist attacks was about 700 between the years 1970 and 1979. This number has dramatically risen to an average of about 25,000 worldwide deaths per year between the years 2010 and 2017 (Global Terrorism Database, University of Maryland). The rise in terrorist attacks beginning in the 1980's fueled substantial research efforts into the blast resistance of windows. Early empirical design procedures based on field blast testing results defined a minimum stand-off distance to prevent failure from a charge of known explosive weight. As more field test data on laminated glass panes were collected, it was realized that a linear interpolation of empirical data to windows of different sizes and aspect ratios other than those already tested led to large errors, as the relationship between the glass window

response and explosive weight is much more complex than a two-variable linear relationship (Zhang et al., 2015). This development led to researchers developing models to give more accurate estimations of laminated glass blast resistant capacities.

In a review of numerical models, Larcher et al. (2012) states the failure process of a laminated glass sheet can be divided into five phases: (1) Elastic behavior of glass plies, (2) Outer glass ply cracks; interlayer is not damaged, (3) Inner glass ply fails; interlayer behaves elastically, (4) Interlayer deforms plastically; splinters are kept together by the interlayer, (5) Interlayer fails at ultimate strength or cut by the glass shards. This is the same process by which laminated glass fails when subjected to blast loading. Extensive research has been conducted on the elastic behavior of laminated glass, making phase (1) possible to model with either analytical or numerical models. However, the complex interaction between the layers makes phases (2) through (5) much more difficult to simulate. Phases (2) through (5) are mostly controlled by the mechanical behavior of the polymer interlayer. Therefore, understanding the dynamic response of interlayer under various loading conditions is critical for developing analytical models that accurately predict the response of laminated glass systems under extreme loading events, such as blast.

One of the earliest models for the failure of laminated glass under uniform pressure is based on the theoretical and experimental research on the bending of laminated glass beams (Hooper, 1973) and the research of nonlinear behavior of glass plates (Vallabhan, 1983). Hooper (1973) found that the bending resistance of laminated glass beams is dependent primarily on the shear modulus of the interlayer. Vallabhan (1983) demonstrated that an iterative approach utilizing von Karmon plate theory could

sufficiently model the behavior of thin rectangular glass plates subjected to lateral pressure. The model, by Vallabhan et al. (1987), consists of two elastic plates modeled by nonlinear von Karmon plate theory connected by an infinitesimally thin elastic shear layer, loaded to large deflections by a uniform pressure (Duser et al., 1999). The model yields a series of differential equations with specified boundary conditions that are solved iteratively using a finite-difference method. Predictions from this model of deflections and stresses have been compared to empirical data measured from strain gauge measurements used in pressure loading tests (Vallabhan et al, 1987). Reasonable data fits were obtained from this model by adjusting the shear modulus of the interlayer and comparing to the specific measurements of the shear PVB at the rate and temperature at which the tests were conducted. However, this model has had little impact on design stands because it limited by its simplifying assumptions. The model assumes linear elastic material properties for the interlayer, failing to capture the strain rate and temperature dependent characteristics associated with polymer viscoelasticity (Duser et al., 1999). Furthermore, the model has not incorporated a glass fracture model into the analysis, which would provide a more comprehensive design method for analysis of laminated glass.

Around the same time, much of the literature reported that the behavior of rectangular laminated glass sections behaved “equivalently” to monolithic glass having the same dimensions at room temperature and under lateral loading lasting 60 seconds and less (Liden et al. 1984; Behr et al. 1985; Behr et al. 1986). These researchers also noted the effects of temperature and interlayer thickness on the fracture strength of laminated glass samples. Minor and Reznik (1990) reported that the fracture strengths of annealed

laminated-glass specimens are equal to fracture strengths of annealed monolithic glass specimens of the same nominal thickness at room temperature, and the fracture strength of laminated glass is reduced to about 75% of monolithic glass at extremely hot temperatures. The researchers describe a theoretical model, often called the LG beam model, which states that the fracture strength and behavior of laminated glass under uniform lateral load always falls between two bounds. The lower bound, termed the *layered* limit, is derived from analysis of two plates which act together but are not connected. The layered limit is approached as the shear modulus of the interlayer approaches zero. The upper bound, termed the *monolithic* limit, assumes the behavior of laminated glass to be equal to that of monolithic glass with thickness equal to the combined thickness of the glass plies, and same geometry. This analysis method essentially ignores the contribution of the interlayer to the fracture strength of the glass.

Current design standards, such as ASTM E1300-03 “Standard Practice for Determining Load Resistance of Glass in Buildings” (2016), utilize this bounded approach of the LG beam method. The standard specifies that the load resistance of glass is determined at the instance of the fracture of any ply in the laminated glass, thus ignoring the post-breakage contribution of the polymer interlayer to the LG system. Therefore, the strength of the laminated glass system lies between the upper monolithic limit and lower layered limit. Despite evidence that the strength laminated glass usually equals or even exceeds that of a monolithic equivalent, this design practice still persists due to uncertainties in the shear response of the interlayer, the role of loading rate and temperature, and the complex nature of a composite material comprised of materials with significant difference in shear and Young’s moduli (Duser et al., 1999). Other standards such as UFC 4-010-01 (2020)

and ASTM F2248-19 (2019) also consider failure of the LG system to be at the instant of fracture of one of the glass plies. UFC 4-010-01 does not specify design procedures, but rather provides baseline criteria for blast resistant glazing such as the minimum interlayer thickness and minimum glazing frame bite and recommends referring to ASTM F2248-19 for design. ASTM F2248-19 is an analytical method based on empirical data that specifies an equivalent 3-second design loading to be used in accordance with ASTM E1300. This method is limited to windows of dimension 6 feet by 8 feet due to lack of testing data on larger sizes. Furthermore, the combined ASTM E1300 and ASTM F2248-19 analysis only applies to laminated glass systems with PVB interlayers.

The advancement of commercially available finite element analysis (FEA) software programs such as ANSYS-AUTODYN and LS-DYNA has enabled researchers to construct complex models that account for the post-breakage behavior of laminated glass systems. Wei et al. (2006) constructed a 3-D nonlinear finite element model to characterize the stress distributions in a rectangular laminated glass sheet with PVB interlayer subjected to hemispherical blast loading using a viscoelastic material model to investigate the role of the interlayer. Duser et al. (1999) utilized a Generalized Maxwell Series to account for temperature and loading rate in the analysis. Their research found that the stress development sometimes fell outside of the monolithic and layered limits prescribed by the LG beam model and that the temperature and loading rate had significant influence in the stress development. The models proposed by Wei et al. (2006) and Duser et al. (1999) demonstrated the efficiency of 3-D FEA models using nonlinear viscoelastic properties for the PVB interlayer by modeling experiments performed by Vallabhan et al. (1993). Other researchers such as Morrison (2007) and Ding et al. (2011)

have studied the application of SDOF and 2DOF models to calculate blast responses of laminated glass panels with PVB interlayers. The SDOF analysis method is also used in UFC 3-340-02 “Structures to resist the effects of accidental explosions”, in which the resistance function is derived from simplifying the time-dependent resistance into two linear portions.

Early numerical models for the behavior of laminated glass only account for pre-cracking behavior, neglecting the post-cracking energy absorption provided by the polymer interlayer. Blast resistant design codes have adopted this simplified analysis and characterize failure of laminated glass at first cracking, failing to characterize the actual resistance of laminated glass under blast loading. Finite element analysis and SDOF/2DOF models have been constructed to account for the post-cracking behavior of laminated glass with PVB interlayer. These models rely on models of the mechanical behavior of the PVB interlayer to accurately approximate the response of laminated glass systems under blast loading. Many researchers have found the behavior of PVB to be very complex and typically highly temperature and strain rate dependent (Bennison 2005; Chen et al. 2018; Liao et al. 2019). More research on the temperature and strain rate effects on the mechanical response of PVB is necessary to further the understanding of the behavior of PVB and to improve existing models of laminated glass subjected to blast loading. Moreover, existing models of laminated glass incorporate PVB as the sole interlayer. In recent years, many emerging polymers such as SentryGlas® have been developed to be used as interlayers in laminated glass systems. More research on the mechanical behavior of these emerging polymers is necessary to accurately characterize their mechanical properties and to develop models for laminated glass systems utilizing

these emerging polymers. In this research, the temperature and strain rate effects on PVB as well as the strain rate effects on SentryGlas® are experimentally evaluated.

2.2 LAMINATED GLASS

Laminated glass comprises two or more monolithic glass layers bonded together with one or more intermediate polymer interlayer such as polyvinyl butyral (PVB) or Sentryglas® (SG) to form a unit. A typical laminated glass system schematic and a laminated glass specimen are shown in Figure 1 (a) and (b), respectively.

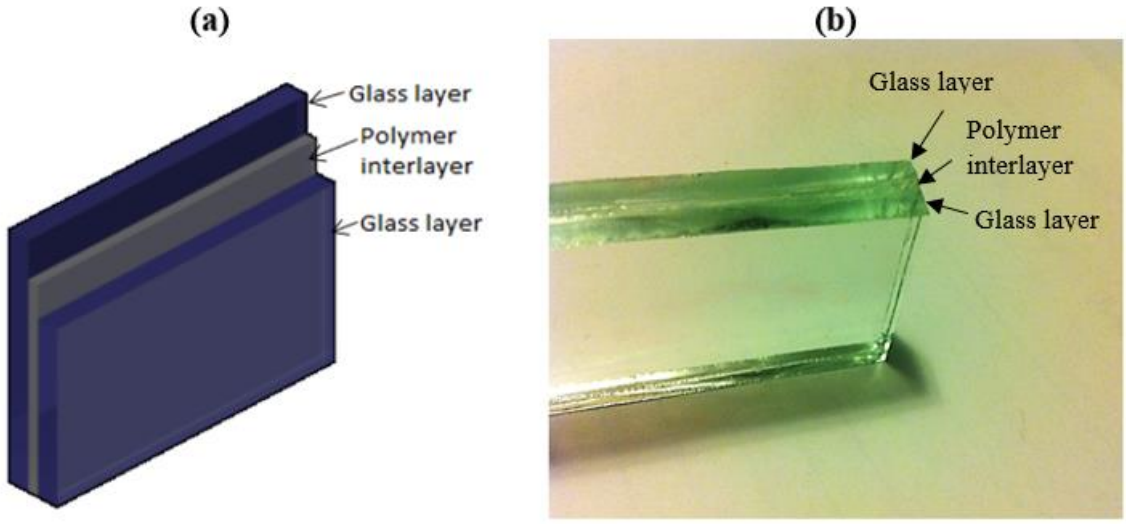

Figure 1: Laminated glass (a) schematic, (b) test specimen.

The glass layers can consist of annealed, heat strengthened, fully tempered, or a combination of glazing types. The bond occurs due to the chemical union between the hydroxyl groups of the polymer interlayer and the silanol groups of the glass layers (Martín et al., 2020). Laminated glass is produced by either the traditional heat and pressure method, or a newer UV curing method. In the heat and pressure method, an

interlayer film is placed between two glass sheets and air is removed typically by vacuum. Large pressure is applied by autoclaves or similar devices and high temperature is applied. Bonding is conducted at temperatures ranging from about 110°C to 140°C (Teotia and Soni, 2014). Resulting laminates retain residual stresses from heat bonding. In the UV curing method, liquid interlayer resin is pumped into the cavity between the glass sheets and is later cured at ambient temperature by exposure to UV radiation. This method is far more cost effective and easier to perform than the heat a pressure method.

Laminated glass was first invented by French chemist Édouard Bénédictus after witnessing a glass flask that had become coated with the plastic cellulose nitrate drop and shatter, but not break into pieces. In subsequent years, laminated glass was patented for use as windshields; however, it did not become widely used until after the invention of polyvinyl butyral (PVB) in 1927 by Canadian chemist Howard W. Matheson and Frederick W. Skirrow. In the mid-1930's United States auto companies discovered that laminated "safety glass" consisting of a layer of polyvinyl butyral between two layers of glass would not discolor and was not easily penetrated during accidents. In the following decade, the new "safety glass" replaced its predecessor and was ubiquitously used as windshields throughout the world.

Today, laminated glass is used for many applications. The primary advantage of laminated glass over monolithic glass is after breakage the polymer interlayer retains the broken glass shards. Laminated glass is therefore advantageous as a safety glazing system in structural applications. In an extreme event such as a hurricane or blast scenario, the polymer interlayer provides post-breakage energy absorption which may prevent flying debris or a blast pressure wave from entering the building, providing occupant safety as

well as minimizing clean-up costs. Laminated glass is also used for bullet proofing applications such as police vehicles as well as increased burglar security. Aside from safety applications, laminated glass is used for noise insulation and solar energy control.

2.3 POLYMER INTERLAYERS: PVB AND SG

Polyvinyl butyral (PVB) is a solid thermoplastic resin. It was first invented in 1927 and has been the standard laminated glass interlayer for the last 70 years. PVB is produced from the reaction of polyvinyl alcohol with butyraldehyde (Martín et al., 2020). The chemical structure is identical for every manufacturer and is shown in Figure *2*. PVB is a random amorphous that consists of three monomers that provide specific properties: hydrophobic and elastic vinyl butyral (~80 weight %) that provides processability, and vinyl alcohol (~18 weight %) and vinyl acetate (~2 weight %) which are hydrophilic and provide high adhesion to inorganic materials such as glass (Roff and Scott, 1971).

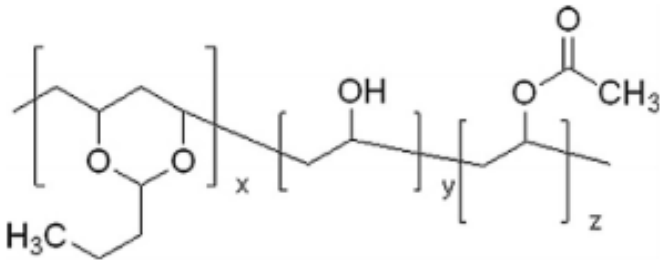

Figure 2: PVB chain structure (Martín et al., 2020).

Even though the chain structure is identical, the specific properties of each PVB sheet depend on the PVB type, manufacturer, and PVB sheet composition. New types of PVB have been recently developed to improve capabilities for specific applications. For

example, Structural PVB is produced with a lower level of plasticizer, which increases its stiffness. Other PVB types include storm and cyclone resistant PVB, acoustic PVB, decorative PVB, and specialized solar PVB that provides solar energy insulation and UV radiation resistance. These specialized PVB sheets are made by altering the sheet properties such as the thickness, sheet composition such as combining two layers or the adding a film layer to produce composite PVB interlayers, or by changing the manufacturing process as in the case of structural PVB. PVB is currently produced and marketed by very few manufacturers worldwide: Eastman (Saflex®), The Kuraray Group (Trosifol® and DuPont®), and Sekisui® (Japan).

SentryGlas® (SG), sometimes referred to as "ionoplast interlayer", is the only commercially available ionomer-based interlayer material for laminated glass. Developed by DuPont for use as structural safety glazing, SG offers much greater rigidity, higher strength, and better ductility (Chen et al., 2020). Since SG was released to market in 1998, structural engineers have commonly used SG as replacement of PVB to improve the mechanical response of laminated glass.

An ionomer is a polymer which has an ionic content of usually no more than 10 mole percent. The general chemical structure of an ionomer, shown in Figure 3, consists of a hydrocarbon containing neutralized pendant acid groups (Weller et al., 2011). SG is formed by a process in which a copolymerization of ethylene with methacrylate is cured with metal ions (Chen et al., 2020). Due to its semi-crystalline chemical structure and crosslinking, SG offers superior mechanical properties compared to traditional amorphous polymer interlayers. Furthermore, SG provides excellent adhesion to glass and metals because of its ionic interactions and chemical union.

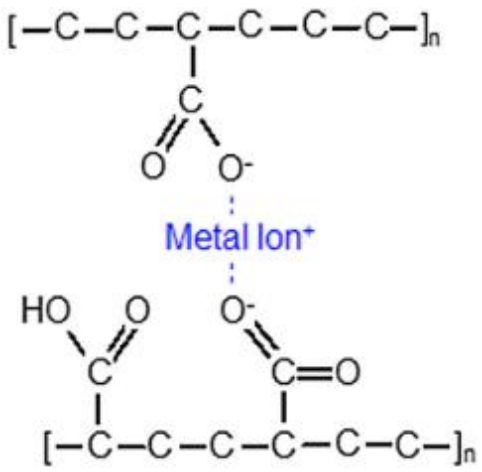

Figure 3: Chemical structure of ionomer (Martín et al., 2020).

With respect to the mechanical performance of laminated glass, the behavior of the polymer interlayer can be split into two phases of interest: before and after glass breakage. Before glass breakage, the interlayer acts to transfer shear force between the plies of glass. This behavior is dictated by the shear modulus of the interlayer. Stiffer interlayer materials, having higher shear (and Young's) moduli, are able to transfer shear forces between the glass plies more efficiently, and therefore perform better before glass cracking than less stiff materials. After glass breakage, the interlayer deforms largely providing post-breakage energy dissipation, while retaining the broken glass shards. In this phase, the ductility, as well as adhesion, of the interlayer material dictates its performance.

However, interlayer polymers are viscoelastic; therefore, their mechanical properties are highly nonlinear, rate-dependent, and temperature dependent. Bennison et al. (2011) performed uniaxial tension tests on virgin PVB and SG and found the strain rate effects are more prominent in the response of PVB compared to SG. At low strain rates, PVB behaves as a hyperelastic material, but as the strain rate increases, the material stiffens

and the response shifts to an elasto-plastic response (Bennison, 2012). SG behaves as an elasto-plastic material regardless of strain rate. The initial response of SG is very stiff until a pseudo-yielding stress is reached, followed by strain softening for some cases, then plastic behavior, and finally strain hardening until failure (Chen et al., 2020). As strain rate is increased, the pseudo-yield stress increases, the strain to failure decreases, and the absorbed energy to failure increases. Strain rate has negligible effect on initial modulus of SG. Chen et al. investigated the temperature effects on PVB (2018) and SG (2020) in direct tension. At the same strain rate, PVB specimens at lower temperatures show elasto-plastic response, while PVB specimens at higher temperatures exhibit hyperelastic behavior. The transition in behavior due to temperature is rather smooth across the four different testing temperatures, with the most noticeable effect being between -5°C (23°F) and 25°C (77°F). For SG tested at the same rate, as temperature increases, the pseudo-yield stress and energy to failure decreases; however, the response is elasto-plastic regardless of temperature.

2.4 STRAIN RATE AND TEST METHODS

In mechanics of materials, strain rate is defined as the rate of change of strain with respect to time. Strain rate is calculated by taking the time derivative of strain, and is usually denoted by the symbol ($\dot{\varepsilon}$). For material testing, most testing types are classified according to the range of strain rates (Figure 4). Quasi-static testing is generally performed at strain rates between 10^{-5} to 10^{-1} s^{-1} utilizing servo-hydraulic testing machines. Servo-hydraulic testing machines carefully control the constant loading rate

through accurate measurement of the displacement of the cross heads. In quasi-static tests, the load is applied at such a low rate that inertial effects can be ignored. High strain rate tests are characterized by strain rates between 10 and 10^4 s^{-1}. Historically, the Split-Hopkinson Bar testing technique was used to achieve high strain rates; however, new age servo-hydraulic machines can achieve high strain rates up to about 1000 s^{-1} (Chen et al., 2020). For intermediate and high strain rate testing, the inertial effects should be considered. The mechanical properties of viscoelastic materials such as interlayer materials are strain-rate dependent; therefore, it is essential to achieve the desired testing strain rates to be able to properly characterize the material properties of such materials.

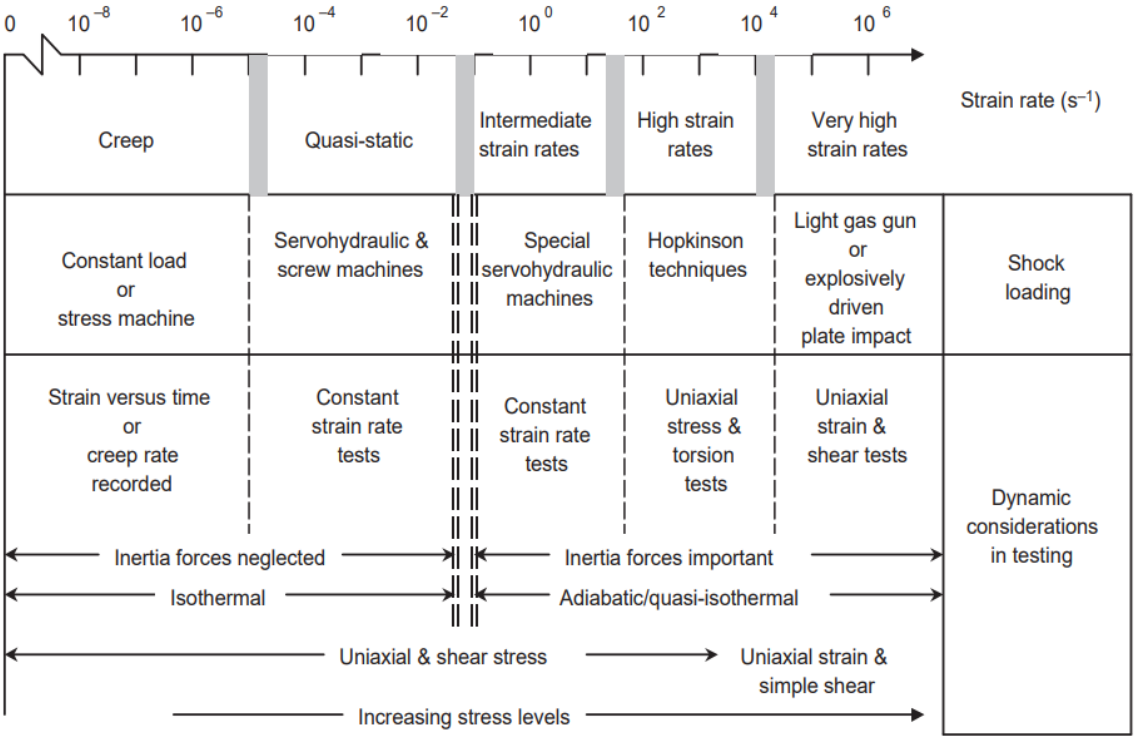

Figure 4: Strain rate regimes and associated instruments and experimental conditions (Nemat-Nasser, 2000).

2.5 QUASI-STATIC TENSILE TESTING

The quasi static tensile test is a method of testing materials in tension under low strain rates. Quasi-static tensile testing is generally performed at strain rates between 10^{-5} to 10^{-1} s^{-1} utilizing servo-hydraulic testing machines. Inertial and stress wave propagation effects are neglected in quasi-static testing because of the extremely low and constant rate of loading. In this research, quasi-static tensile testing of interlayer polymers was performed according to ASTM D638-10 Standard Test Method for Tensile Properties of Plastics (2010) utilizing a servo-hydraulic testing machine.

2.6 DROP WEIGHT TESTING

Drop weight testing is a testing method to achieve high strain rates without the use of a servo-hydraulic testing machine. In this method, a known weight is dropped in vertical free fall along guiding pipes. Attached to the weight are strikers which impact an anvil attached to the bottom of the material specimen, pulling the specimen in tension at high strain rates. The top of the specimen is attached to a dynamic load cell which collects the load-time history. Prior to testing, the gage length is marked onto each specimen. A high-speed camera is utilized to record the elongation of the specimen. The strain-time history can then be derived using digital image coordination software. The impact energy can be calculated using principles of kinematics and energy conservation. Effects of friction and air resistance can be accounted for by comparing numerical methods to empirical data.

Drop weight testing has been performed for the characterization of material properties by several research teams. Aymerich et al. (1996) utilized a drop weight testing method to study the material properties of emerging composite materials. Kliner et al. (2009) developed a drop-weight testing instrument to obtain flow curves of AA5754 aluminum at strain rates of up to 2,200 s^{-1}, and the results were verified through simulations using commercial FE code LS-DYNA.

For this research, drop weight tests were performed using an existing drop weight machine presented in Chapter 3.

CHAPTER 3 - EXPERIMENTAL DESIGN AND SETUP

3.1 INTRODUCTION

In this Chapter, all experimental designs are presented. Specimen preparation for quasi-static and drop weight test specimens is discussed in Section 3.2. A detailed description of the drop weight test apparatus, drop weight data collection and analysis procedures, as well as a drop weight dynamic model are presented in Section 3.3. The quasi-static test setup and data acquisition system is detailed in Section 3.4.

3.2 SPECIMEN PREPARATION

In this research, all specimens tested were cut from virgin, or prelaminated, interlayer materials following ASTM 638-10 (2010) standard. Aged PVB, unaged PVB, and SG specimens were experimentally evaluated. The aged PVB tested in this research is Saflex® Clear PVB (RB71), 0.05-inch thickness, provided by Eastman. This material was left over from previous research conducted in 2015. The PVB was stored in a temperature-controlled room, but was subjected to sunlight which resulted in light discoloration (Figure 5).

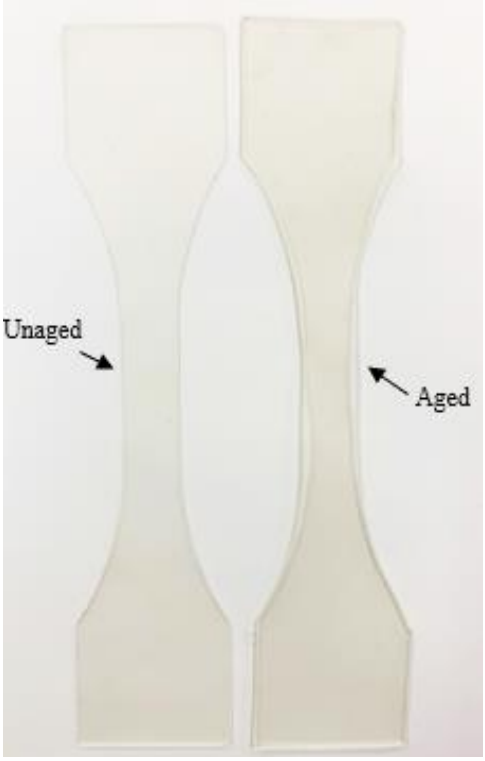

Figure 5: Aged and unaged PVB specimens.

The unaged PVB is Saflex® Standard Clear PVB (RA41), 0.03-inch thickness, provided by Eastman. The SentryGlas® tested in this research is SentryGlas Xtra (SGX) Ionoplast (SG6000), 0.06-inch thickness, provided by Kuraray.

3.2.1 Drop Weight Testing Specimen

The drop weight testing specimen geometry was designed based on ASTM D638-10 (2010) standard Type I specimen, shown in Figure 6a. However, specimen geometry was modified to increase the bonding area between the aluminum end tabs and the interlayer polymer specimens in order to prevent the tearing out of the specimens at the ends (Nawar, 2016). This modified geometry is shown in Figure 6b.

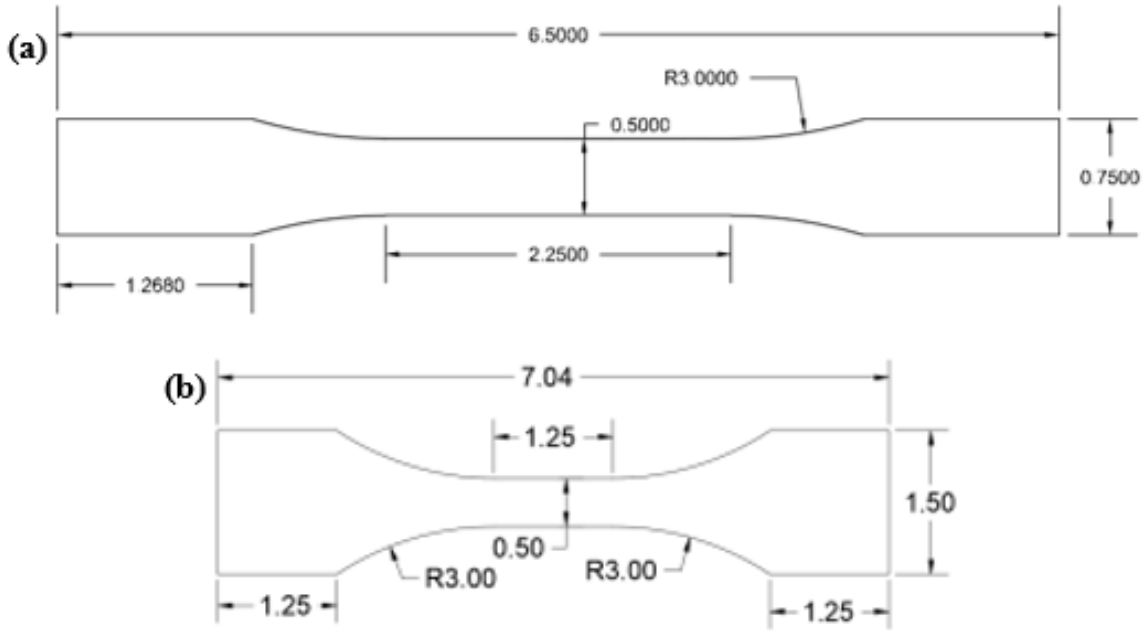

Figure 6: (a) Unmodified and (b) modified (N.T.S) ASTM Type I specimen geometry.

To ensure the accuracy of the specimen dimensions, a steel cutting die was manufactured (Figure 7a). The cutting die was used to stamp the specimens using arbor press (Figure 7b). A central gage length of 1 inch was marked with two dots using a permanent marker pen. To ensure accuracy of the gage length, a specialized aluminum template was utilized (Figure 8). Digital calipers were used to measure the thickness and width of the gage length at three locations to an accuracy of 0.0005 inches. Finally, aluminum end tabs, with dimensions 1.25 in. × 1.50 in. × 1/16 in., were superglued onto the front and back of each end, and the interlayer material between the holes in the tabs was punched out. A fully prepared drop weight test specimen is shown in Figure 9.

Figure 7: Drop weight specimen preparation; (a) cutting die, (b) specimen stamping.

Figure 8: Gage length template.

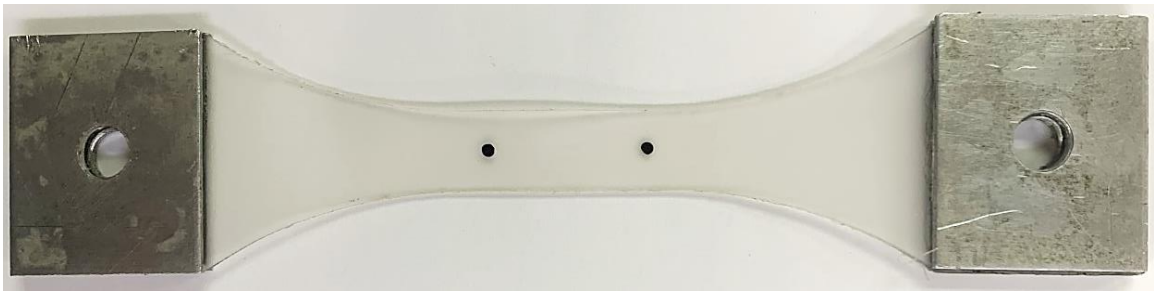

Figure 9: Drop weight test specimen.

3.2.2 Quasi-Static Testing Specimen

The quasi-static testing specimen geometry was chosen according to ASTM D638-10 (2010) to be a standard Type IV specimen geometry (Figure 10). Specimens were stamped using a steel cutting die (Figure 11). The quasi-static test specimens did not require end tabs to prevent tearing out or slippage during testing. Prior to testing, a gage length of 1 in. was marked with two dots using a permanent marker pen onto each specimen.

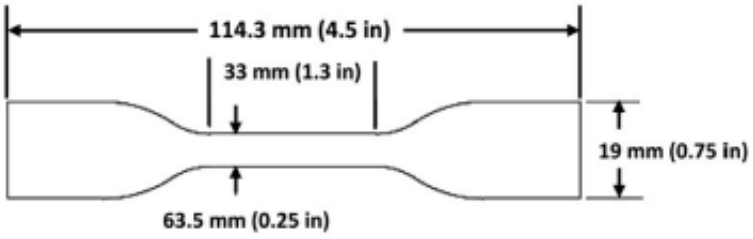

Figure 10: Quasi-static specimen geometry.

Figure 11: Quasi-static specimen cutting die.

3.3 DYNAMIC DROP WEIGHT TEST SETUP

In this section, the drop weight testing machine will be described in detail. The data acquisition system and general data analysis procedure will be discussed. Also, a drop weight testing dynamic model will be presented.

3.3.1 Drop Weight Testing Apparatus

The high strain rate tensile testing was performed using the drop weight testing machine shown in (Figure 12a). This device was originally designed for impact testing of hard materials such as metals or composites. In order to perform high strain rate tests on polymers, several new parts were designed, manufactured and installed. A schematic of the machine with the critical members labeled is shown in (Figure 12b).

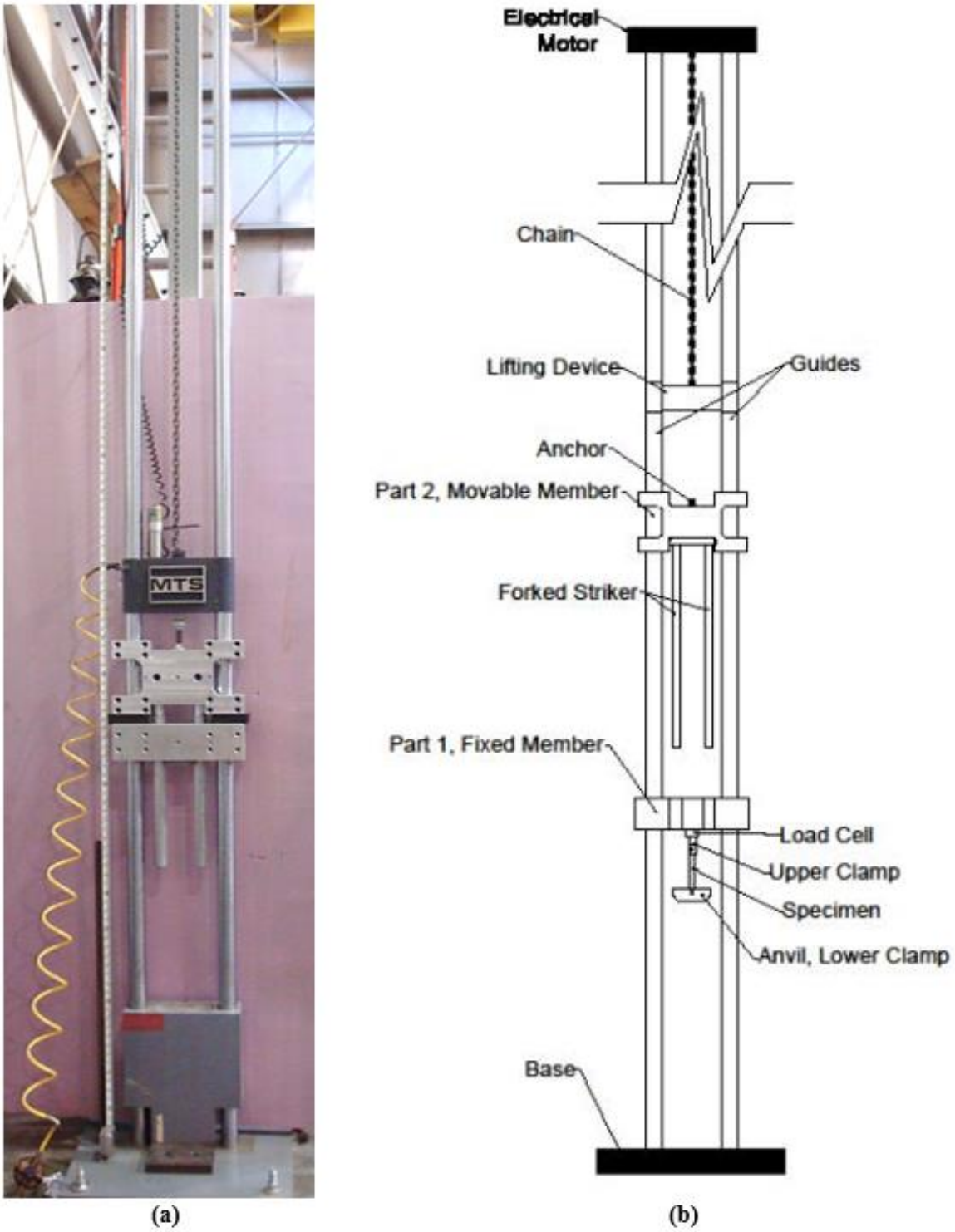

Figure 12: Drop weight testing machine. Say what is (a) and what is (b)

3.3.1.1 Fixed Member, Part 1

The fixed member shown in is a two-part aluminum plate of plate of dimensions 14 × 4 × 4 inches. The main function is to hold the load cell which is attached to the bottom of the fixed member by threaded connection. The member also stops the weight after the specimen is tested. Two through holes of 1.5 in. diameter allow the striker to pass through the fixed member.

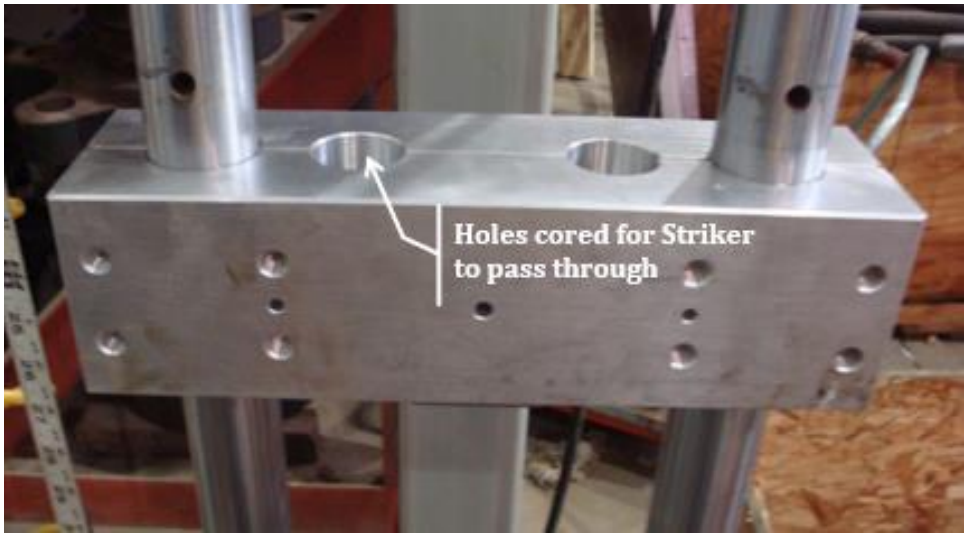

Figure 13: Fixed member, Part 1.

3.3.1.2 Moveable Member, Part 2

The moveable member, along the attached forked striker, is the drop weight itself (Figure 14). It is an x-shaped aluminum plate with overall dimensions (sans cutouts) of 14 × 8 × 4 inches. The weight of the moveable member is 28.7 pounds. The top of the moveable member is designed for additional weight to be added. The moveable member is free to slide vertically along the guide rails. Attached to the bottom of the moveable member is

an aluminum plate (not shown in Figure 14) to which the forked striker is attached. The moveable member is retrieved and brought to the desired drop height by the lifting device.

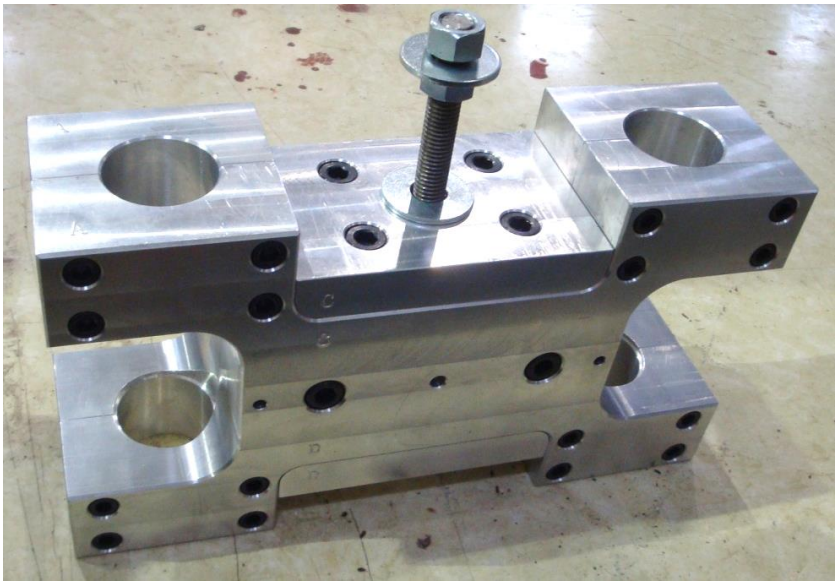

Figure 14: Moveable member, Part 2.

3.3.1.3 Striker

The striker consists of two hollow aluminum rods of 1.5 in. diameter and 27.5 in. length attached to an aluminum plate of dimensions 6 × 4 × 1 inches through threaded connections (Figure 15). The striker is attached to the moveable member through bolted connection. The length of the striker allows for a large “stroke” length which assures breakage of the elastic testing materials. This stroke length can be adjusted by increasing or decreasing the number of 1 in. thick rubber pads that are set on top of the fixed member which act to stop the moveable member. The total weight of the striker is 3.4 pounds.

Figure 15: Striker.

3.3.1.4 Clamps

Two clamps are used in the drop weight setup to hold the test specimen. The upper clamp, shown in Figure 16, consists of two steel parts: one is an L-shaped part which is attached directly to the bottom of the load cell through a threaded connection, and the other is a small steel plate of dimensions 1.25 × 1.25 × 0.5 inches which is the front face of the clamp. A 3/8-inch diameter bolt is used to clamp the top end of the testing specimen between the front face part and the back of the L-shaped part of the upper clamp.

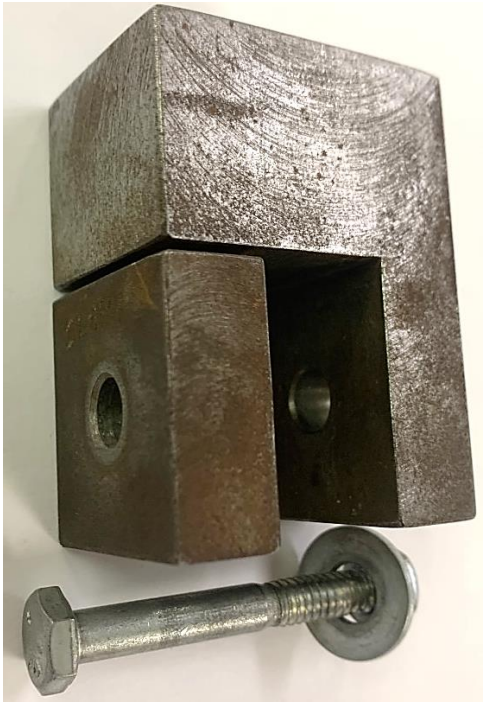

Figure 16: Upper clamp for clamping the test specimen.

The lower clamp, or the anvil, is attaches to the lower end of the specimen, and receives the impact of the striker. Because this clamp is applied directly to the test specimen, the anvil was made of aluminum to minimize pre-tensioning of the test specimens. The anvil consists of two aluminum plates, each of 0.95-inch thickness, connected by one 5/16-inch diameter bolt in the center (Figure 17). In order to prevent the individual plates from rotating, one of the aluminum plates has pegs which snuggly fit into holes in the other peg (Figure 18). This provides rigidity and allows efficient transfer of force to the test specimen. The anvil has recessed circles on the top to receive the forked striker, reducing any rebound effect. The total weight of the anvil and bolt connection is 2.02 pounds.

Figure 17: Bottom clamp (anvil).

Figure 18: Anvil pegged connection.

3.3.1.5 Load Cell

The load cell used was a dynamic piezoelectric load cell with a capacity of 500 pounds (Omegadyne model LC213-500). The upper end of the load cell was connected to the fixed member and the lower end of the load cell was connected to the upper clamp. This connection is shown in Figure 19.

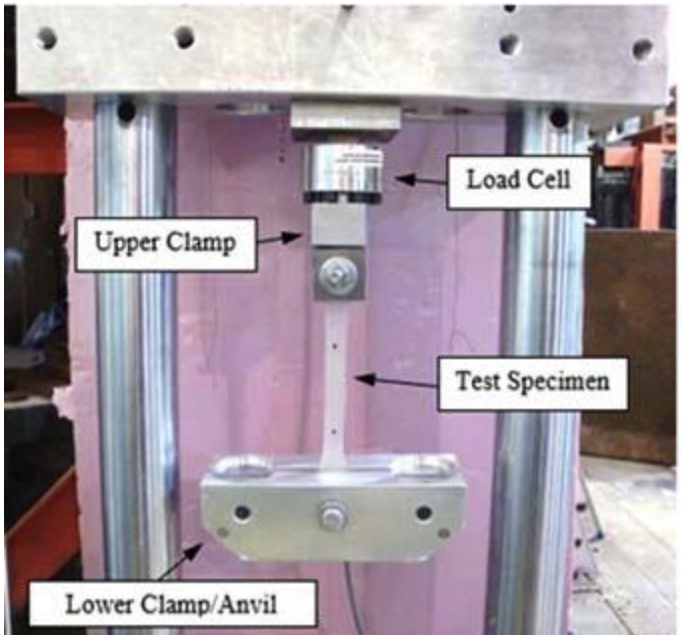

Figure 19: Load cell connection.

3.3.2 Dynamic Data Acquisition System

The load readings from the load cell were recorded through a specially designed drop weight Lab View program by a Nation Instruments USB-6351 data acquisition system. The drop weight Lab View program collects a large sample of data in one big, continuous loop, only writing the data once the test is complete. For high speed tests, it is essential that all of the data is collected in one singular loop, so that no data is missed by writing the data. The interface of the drop weight program is shown in Figure 20.

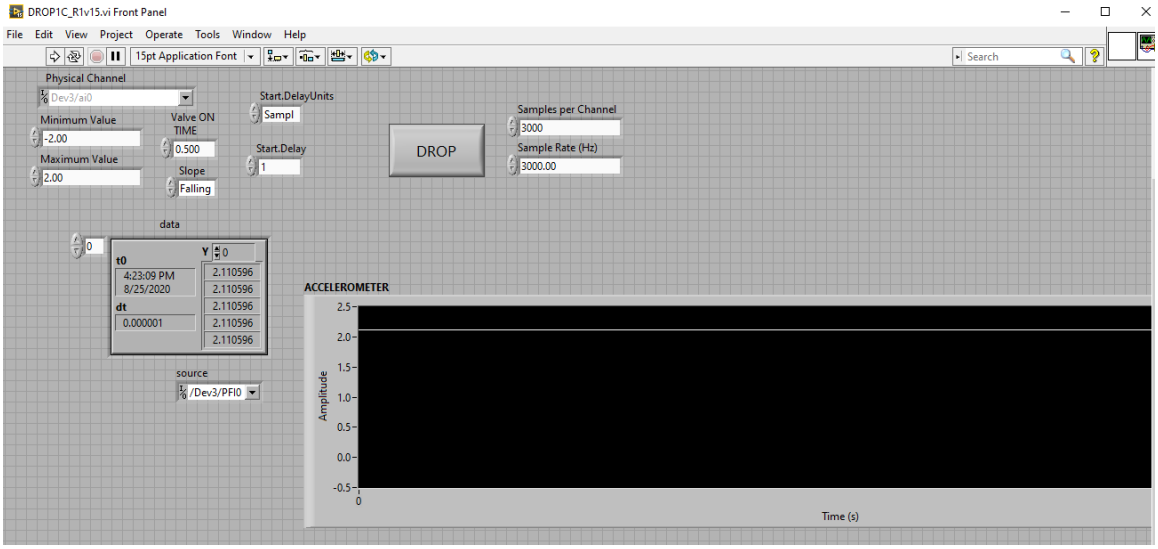

Figure 20: Drop weight Lab View data acquisition program.

3.3.3 High-Speed Photography

In high strain rate testing, recording strain is one of the major obstacles. The use of mechanical extensometers or strain gages is impractical as they would be damaged due to inertial effects, or impact in the case of drop weight testing. In order to determine the strain in the material, a high-speed camera with a maximum frame rate of 20,000 frames per second was used to record the test. The specific camera used in this test setup was an edgertronic® model SC1 camera show in Figure 21, and the highspeed videos were collected at a rate of 3000 per second. The video from the high-speed camera was then converted into a file of sequential pictures of each frame, and digital image correlation software was used to calculate strain-time history.

Figure 21: High-speed camera.

3.3.4 Dynamic Data Analysis

After performing a drop weight test, the load history was obtained from the Lab View program. Load was converted to engineering stress by dividing by the original cross-sectional area of the gage length.

In order to determine the strain history, the video from the high-speed camera was converted to images of each frame. Unnecessary frames before impact and after failure were deleted. The file of pictures was then uploaded to a Photo Track software program, developed for this research, which tracks the displacement, velocity, and acceleration of two specified pixels between pictures. To begin analysis, pixels in the center of each gage length dot marking were chosen (Figure 22). The program tracks these pixels through the last picture of the file, and the displacement, velocity, and acceleration of the specified pixels is written to a text file. From the displacement of the gage length dots, the engineering strain-time history was derived by setting the initial distance between the

chosen pixels equal to the known initial gage length of 1 inch, and setting the change in time between frames equal to the frame rate of the camera.

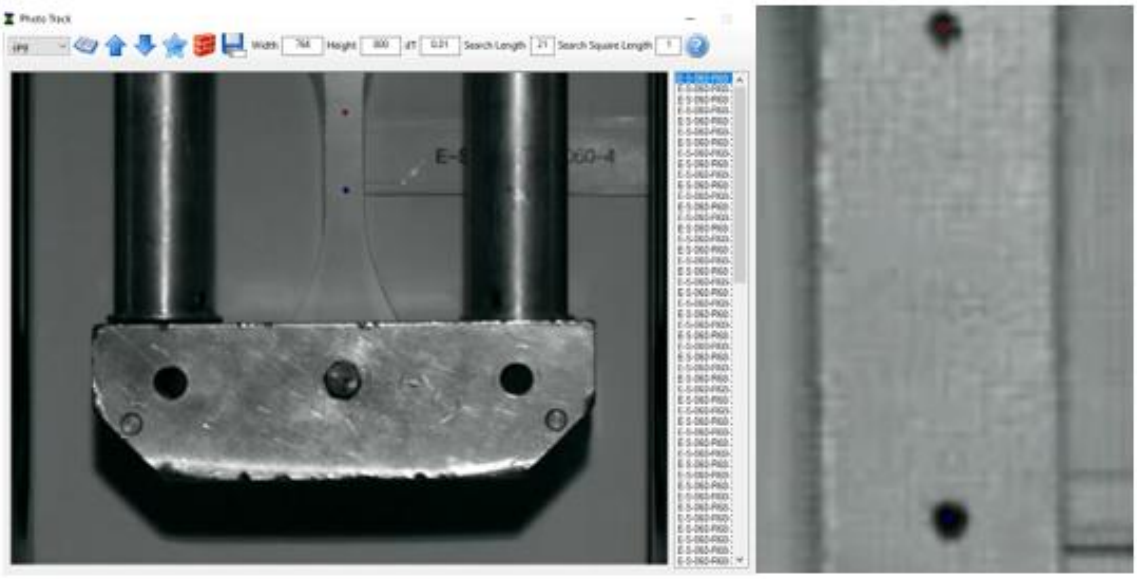

Figure 22: Photo Track software gage length.

3.3.5 Drop Weight Dynamic Model

The strain rate of the drop weight machine can be adjusted by changing the drop height. In order to determine a reliable method to estimate the strain rate value, it is an essential step to first model the dynamic impact of this apparatus (Figure 23a). There are several parameters related to the dynamic system that should be quantified, such as the weight of the dropped mass (m_2), the anvil mass (m_1), the height of the dropped weight (H), as well as other important parameters. The following equation was used to simulate the system (Chopra 2012).

$$\dot{u}(t) = -A\,\omega_n \sin(\omega_n t) + B\,\omega_n \cos(\omega_n t)$$

$$\omega_n = \sqrt{\frac{k}{m}} \qquad \text{Eq (1)}$$

Where $\dot{u}(t)$ is the speed, t is the time, ω_n is the natural frequency of the system, A and B are constants, k is the specimen stiffness, and m is the system mass.

A finite element (FE) model was created to calculate the stiffness and strain of this geometry. Ansys FE code (ANSYS 2017) was used to generate the mesh, Figure 23b. A linear elastic isotropic material model was used to simulate the specimen. It was found that the normalized stiffness of this geometry is equal to $0.14E\times th$, where E and th are Young's modulus and thickness of the specimen, respectively. In addition, the strain within the gage length zone (L_g) was found to be 1.32 times the strain in the overall zone between the grips (L_t), as seen in Eq 2.

$$\varepsilon = C_1\,\varepsilon_O \qquad \text{Eq (2)}$$

Where ε_O is the average strain over the total free length of the specimen (L_t), ε is the strain at the gage length zone (L_g), and C_1 is a correction factor calculated to be 1.32. A code was written to model the dynamic system shown in Figure 23a to determine the values of parameters needed to produce the target strain rate.

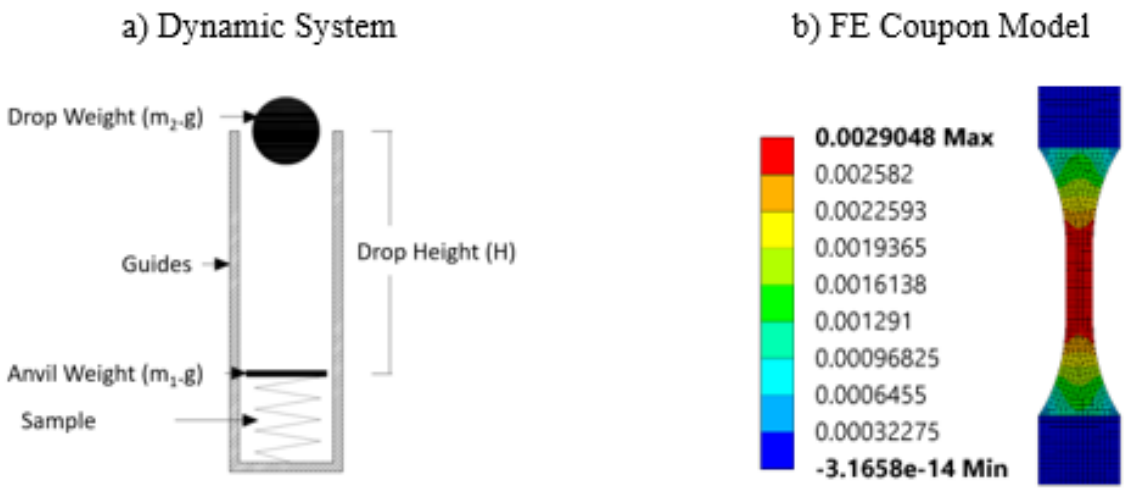

Figure 23: Dynamic system model of drop weight machine.

Assuming a full plastic impact, i.e., the anvil and drop weight will stick together, and applying the boundary conditions will lead to the following equation for the average strain rate ($\dot{\varepsilon}_{av}$) over time from 0 to t:

$$\dot{\varepsilon}_{av}(t) = \frac{C_1 C_2}{t.L_g}\left[2\frac{m_2 g}{k}\sin^2\left(\frac{\omega_n t}{2}\right) + \frac{\left(m_2\sqrt{2gH}\right)}{\omega_n(m_1+m_2)}\sin(\omega_n t)\right] \quad \text{Eq (3)}$$

Where g is the gravitational acceleration and C_2 is a calibration coefficient evaluated from experimental results to incorporate the friction and wind resistance losses as well as the instrumentation and measurement devices errors. The height required to produce a specific strain rate value can be evaluated from the following equation.

$$H = \frac{1}{2g}\left[\frac{\omega_n(m_1+m_2)}{m_2\sin(\omega_n t)}\left(\frac{t.L_g}{C_1 C_2}\dot{\varepsilon_{av}}(t) - 2\frac{m_2 g}{k}\sin^2\left(\frac{\omega_n t}{2}\right)\right)\right]^2 \quad \text{Eq (4)}$$

The calibration and verification for this model will be discussed in Chapter 4.

3.4 QUASI-STATIC TEST SETUP

Quasi-static testing was performed utilizing a ADMET servo-hydraulic testing machine (model eXpert 2611) shown in Figure 24a. The device is equipped with a load cell with a capacity of 2000 pounds. The load was recorded on a Lab View program designed for quasi-static testing of polymers. The displacement rate of the cross-heads was set to be 2 inches per minute following ASTMK D638-10 standard (2010). A Microsoft Azure Kinect DK 1880 PC Peripheral camera with a rate of 30 frames per second was used to record the strain of the specimen during testing (Figure 24b). The strain-time histories were produced using the same digital image correlation process described in Section 3.3.4. The only difference is that the video was converted to frames at 1 second intervals due to the long duration of the tests, some lasting more than five minutes. All quasi-static tests were performed at room temperature (68°F-72°F). A PVB specimen being tested is shown in Figure 24c.

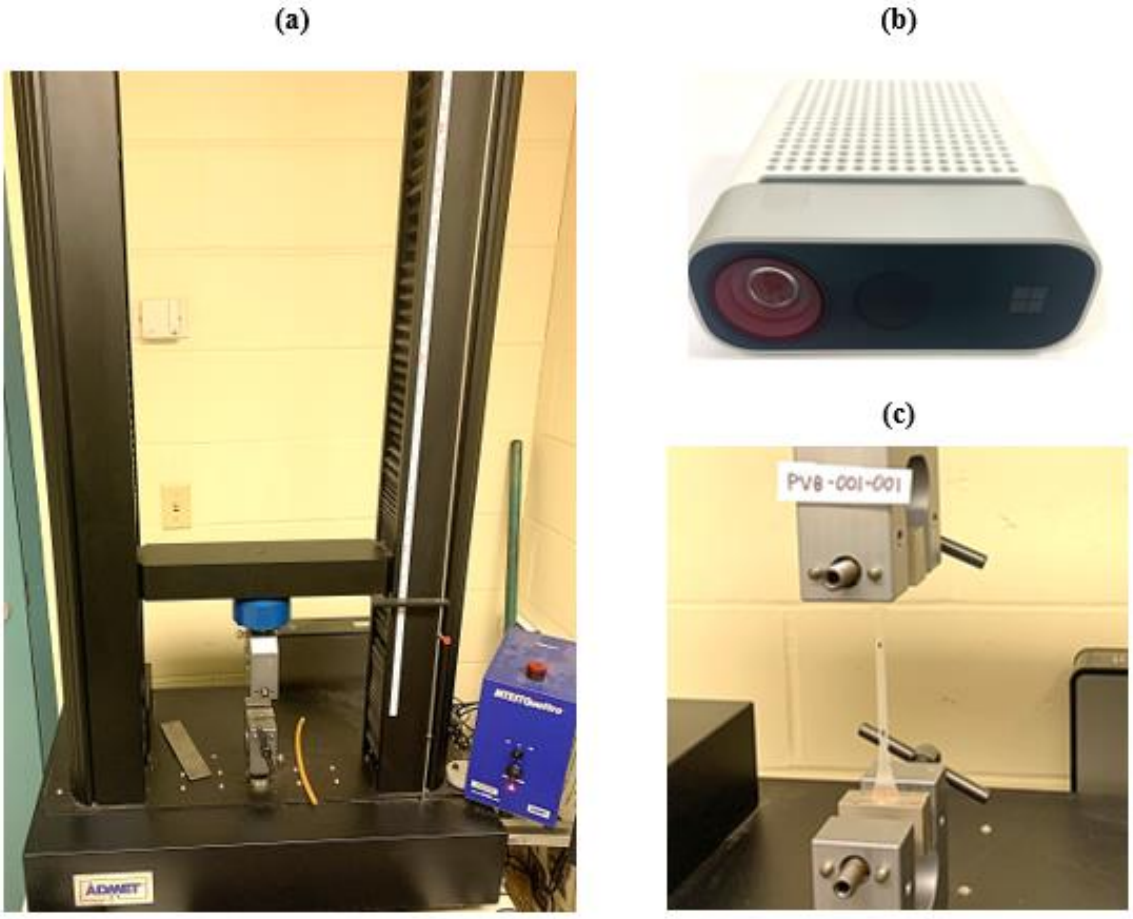

Figure 24: Quasi-static test setup: (a) test machine, (b) camera, (c) quasi-static testing of PVB specimen.

CHAPTER 4 - DYNAMIC AND STATIC EXPERIMENTAL EVALUATION

4.1 INTRODUCTION

In this chapter the experimental results of four studies are presented: drop weight testing of aged PVB (Section 4.2), drop weight testing of unaged PVB at various temperature ranges (Section 4.3), drop weight testing of SG (Section 4.4), and quasi-static testing of unaged PVB and SG (section 4.5). For each study, the engineering stress-strain responses will be discussed. Plots discussed in this chapter show the curve of five test specimens, with the individual test data represented with markings.

4.2 DROP WEIGHT TESTING OF AGED PVB

In this study, six testing groups were performed. Aged PVB specimens of 0.05 in. thickness were tested using the drop weight machine with drop heights ranging from 6 to 64 inches. Tests were performed at each drop height until five valid tests were achieved. A test was considered invalid if the failure of the specimen did not occur within the gage length. Three tests were performed at the maximum drop height of 64 inches in order to determine the maximum achievable strain rate of the unmodified drop weight test setup. The main objectives of this initial study were to validate and calibrate the drop weight dynamic model, and to study the strain rate effect on aged PVB. In this section, the results of the six groups will be presented.

4.2.1 Results and Discussion

The results presented will include the engineering strain-time histories, engineering stress-strain relationships, and a discussion of the strain rate effects. Also, the validation and calibration of the drop weight dynamic model will be discussed. The tests performed in this study were not temperature controlled and were performed at a range of relatively hot temperatures. For each test group, the average temperature was recorded.

4.2.1.1 Strain-Time Histories A typical engineering strain-time response for a PVB drop weight test is shown in Figure 25. In general, the strain-time response is linear; however slight softening occurs after about t = 0.01 sec. Therefore, the experimental strain rate, $\dot{\varepsilon}_E$, was calculated as the slope of the tangent to the initial linear portion of the strain-time curve at t < 0.001 sec.

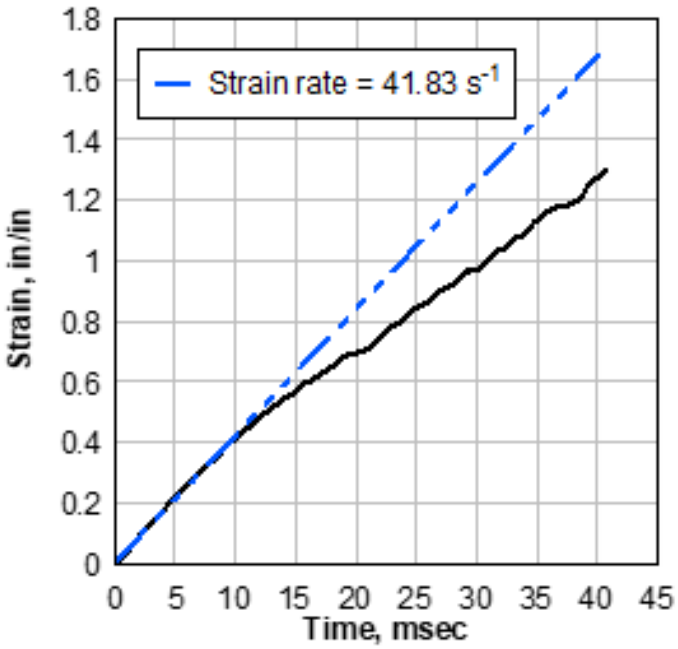

Figure 25: Typical engineering strain versus time curve for PVB drop weight specimen.

The strain-time histories for each of the six testing groups are shown in Figure 26. For the drop height H = 6 in., the specimens did not fail, which resulted in an uncharacteristic, severely bilinear strain-time response shown in Figure 26a. The specimens strained linearly for t < 150 msec under the initial impact of the drop weight, regained strain as the weight rebounded, and then strained at a very low rate while supporting the weight for the duration of data collection. Because the specimens did not fail, this test group is invalid, and was not considered in the comparison of the experimental strain rate results to the predicted strain rates of the analytical model. The results of the drop heights 18 in. through 64 in. are shown in Figure 26b through Figure 26f. The curves are generally considered linear; although slight softening occurs after about t = 10 msec. The strain to failure is about 1.4 in/in for each drop height. As the drop height increases, the experimental strain rate increases, and the time to failure decreases.

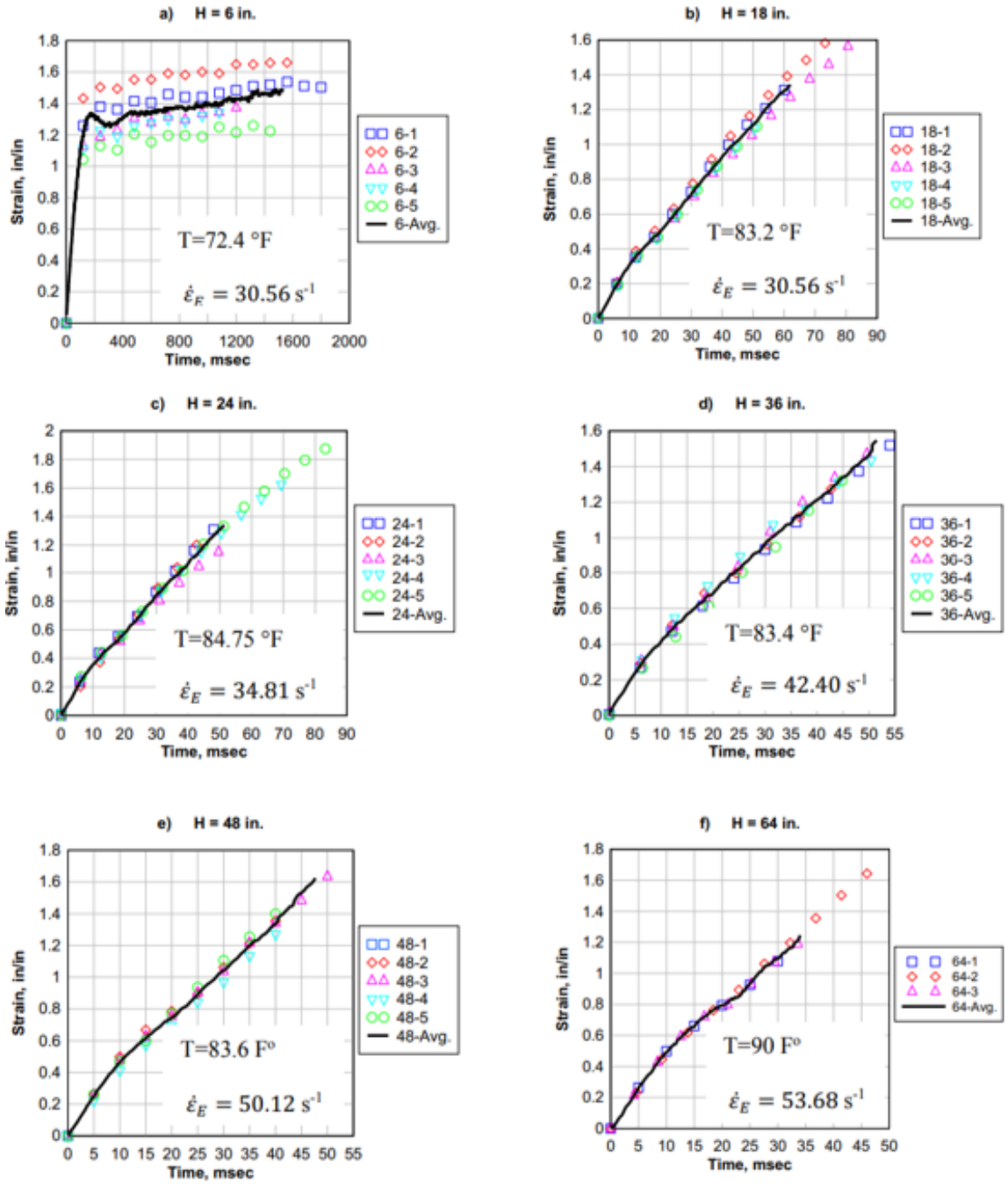

Figure 26: Engineering strain-time histories of aged PVB.

4.2.1.2 Validation and Calibration of Drop Weight Testing Dynamic Model

The strain-time histories were used to validate the analytical model of the drop weight machine, and to calibrate it to accurately predict drop heights to achieve desired strain rates for future testing. The experimental strain rate for each drop height was calculated as the slope of the tangent line of the average strain-time curve for the initial linear portion of t < 10 msec. The results show that the drop height significantly affects the strain behavior. Table 1 shows a comparison between the experimental average strain rates and the predicted average strain rates from the analytical model at t < 10 msec. It can be found that the model was able to predict the strain rates closely. is a plot of the experimental vs. analytical strain rates. The calibration coefficient was determined to be equal to $C_2 = 0.96$.

Table 1: Comparison between experimental and analytical strain rates of aged PVB drop weight study.

Drop Height (H), in.	Average Testing Temperature, °F	Initial Strain Rate, s^{-1}		
		Experimental	Analytical	Percent Difference, %
18	83.2	30.29	30.56	+0.88
24	84.75	34.81	35.21	+1.14
36	83.4	42.40	43.01	+1.43
48	83.6	50.12	49.58	-1.07
64	90.0	53.68	55.27	+2.90

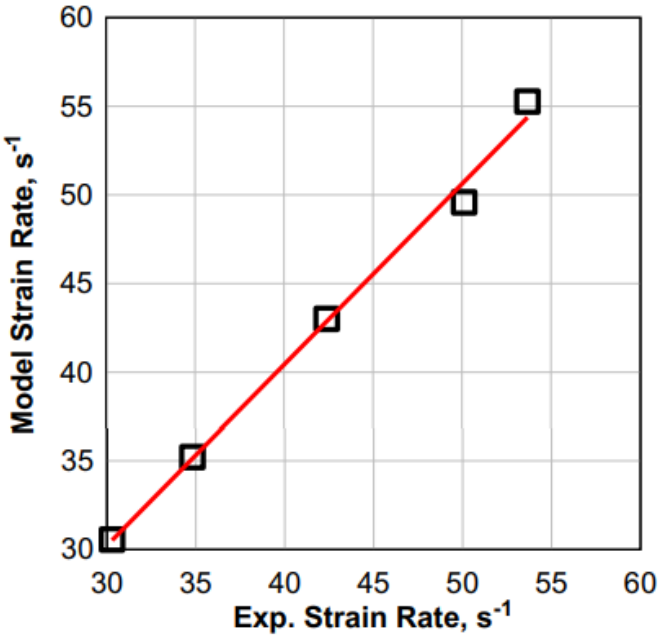

Figure 27: Comparison between experimental and analytical strain rates

4.2.1.3 Stress-Strain Behavior

A typical engineering stress versus engineering strain response for a PVB specimen drop weight test is shown in Figure 28. The stress shows a steep initial rise until a turning point after which the increase in stress slows down. The stress–strain curve depicts typical elasto-plastic like behavior. However, the drop in modulus is not an actual sign that the material has yielded. Almost all the elongation of the specimens was recovered after failure (Figure 30). This indicates that despite an elasto-plastic like, or bilinear, behavior, the extension in PVB is viscoelastic rather than plastic. For easy demonstration of PVB mechanical behavior at high strain rate, a pseudo-yield stress $\sigma_{ps,y}$, where material modulus changes abruptly, and the corresponding strain, pseudo-yield strain $\varepsilon_{ps,y}$, are defined. The failure stress, σ_f, and corresponding strain to failure, ε_f, are calculated at the

time when the specimen fractured. Two moduli are considered, the initial modulus, E_{ini}, which is defined as the slope of the initial linear response through the pseudo-yielding point, and the secondary modulus, E_{sec}, which is defined as the slope of the second linear portion of the bilinear response after pseudo-yielding point. The strain energy to failure, U, is calculated as the total area under the engineering stress-strain curve.

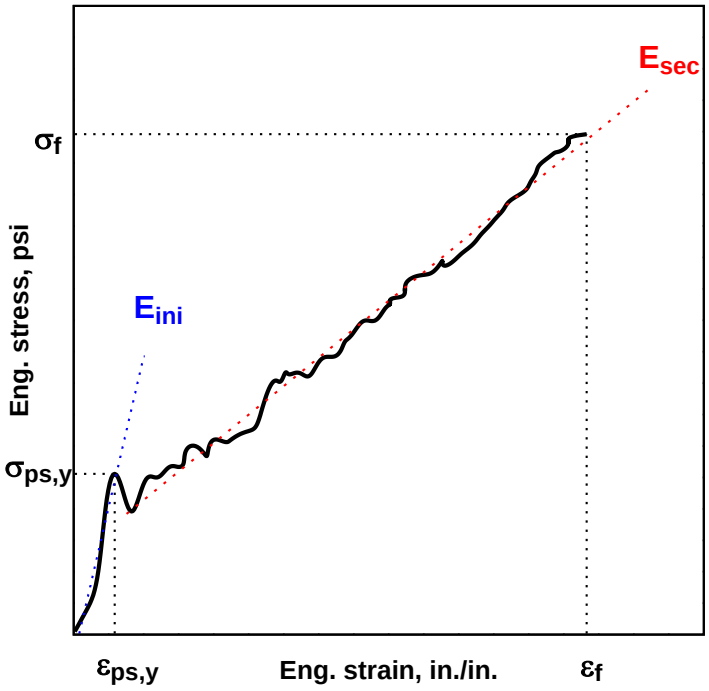

Figure 28: Typical aged PVB engineering stress versus engineering strain data analysis

The engineering stress versus engineering strain curves for the PVB specimens are shown in Figure 29. A summary of the average results for each drop height testing group is presented in Table 2. The testing results for each are summarized in Table 3.

As the drop height was raised from 6 in. to 48 in., the strain rate increases from 13 to 50 s^{-1}. The increase in strain rate significantly affects the initial linear elastic response. Both

the pseudo-yield stress and the initial modulus increase with the increase in strain rate. Therefore, as the strain rate increases, aged PVB becomes stiffer and stronger until the pseudo-yielding point. The pseudo-yield strain shows no discernable dependence on strain rate. The secondary modulus also increases with strain rate, although the effect of strain rate on the secondary modulus is not as significant as it is on the initial modulus. The average failure strain for all of the tests was between 1.35 and 1.53, with no noticeable relationship with strain rate. The failure stress and strain energy to failure both increase with increase in strain rate.

For the drop height of 64 inches, the strain rate is 53.8 s^{-1}. The results of this testing group largely resemble the results of the testing group for the drop height of 48 inches. The failure stress, failure strain, secondary modulus, and strain energy are very similar; however, the initial linear responses differ greatly. The pseudo-yield stress, pseudo-yield strain, and initial modulus are significantly reduced for the drop height of 64 inches. The reduction in initial stiffness and strength is likely due primarily to the increase in temperature. Previous studies on the temperature effect on viscoelastic interlayers have shown at lower temperatures, the elastic component of the response is predominant, and at higher temperatures, the viscoelastic component is predominant (Liao et al. 2019; Chen et al. 2020).

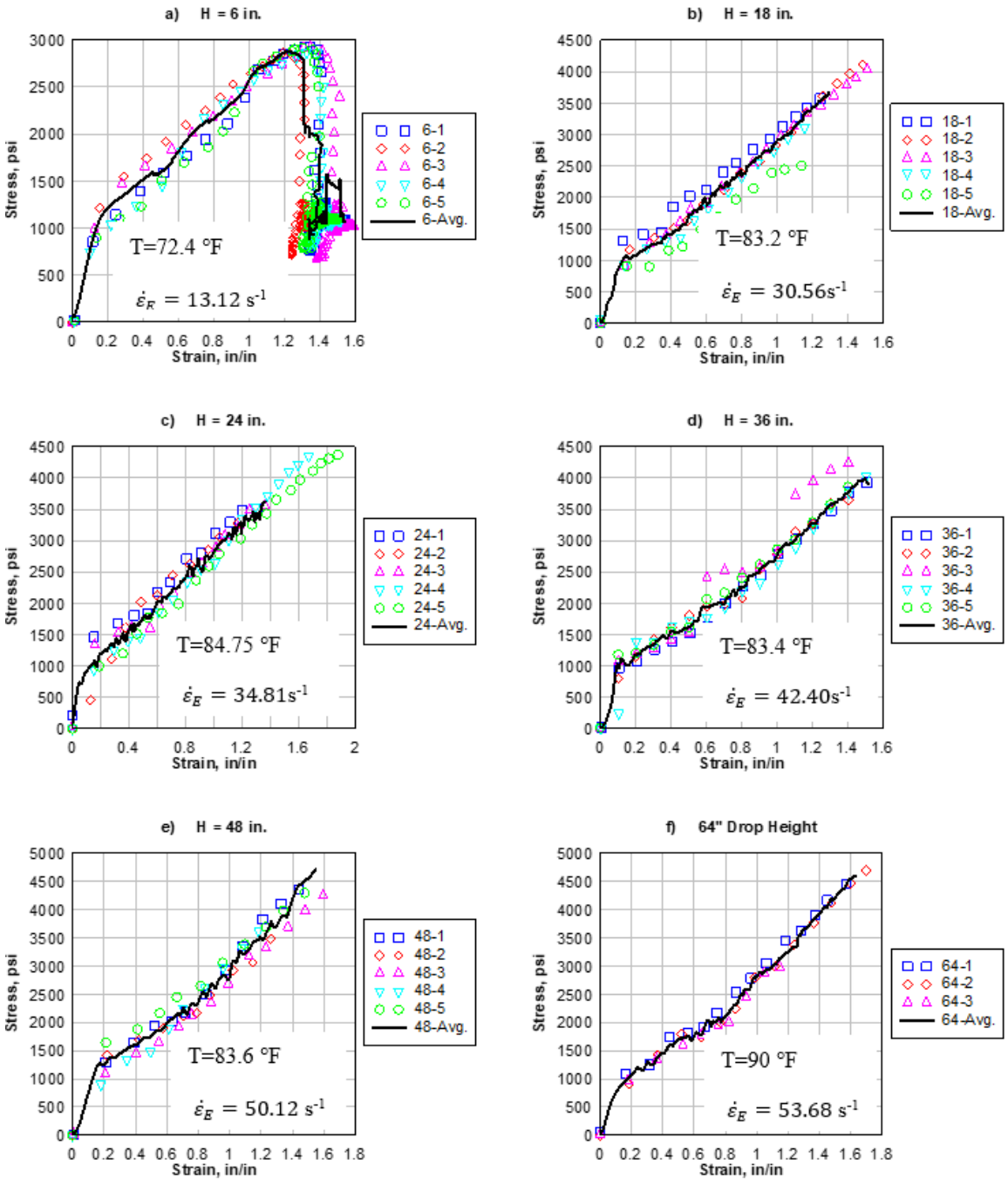

Figure 29: Engineering stress vs. engineering strain of PVB at various strain rates.

Table 2: Summary of aged PVB drop weight test results.

Drop Height (in)	Avg. $\dot{\varepsilon}_E$ (s^{-1})	Avg. Eng. $\sigma_{ps,y}$ (psi)	Avg. Eng. $\varepsilon_{ps,y}$ (in/in)	Avg. Eng. σ_f (psi)	Avg. Eng. ε_f (in/in)	Avg. E_{ini} (psi)	Avg. E_{sec} (psi)	Avg. U (psi·in/in)
6	13.17	1164	0.174	2907	1.512	7630	1684	2800
18	30.56	1072	0.109	3516	1.348	11020	2249	2827
24	34.81	1171	0.078	3936	1.518	11479	2119	3563
36	42.40	1223	0.129	3996	1.460	13443	2332	3253
48	50.12	1231	0.149	4264	1.504	12407	2443	3616
64	53.68	777	0.103	4171	1.527	8124	2407	3512

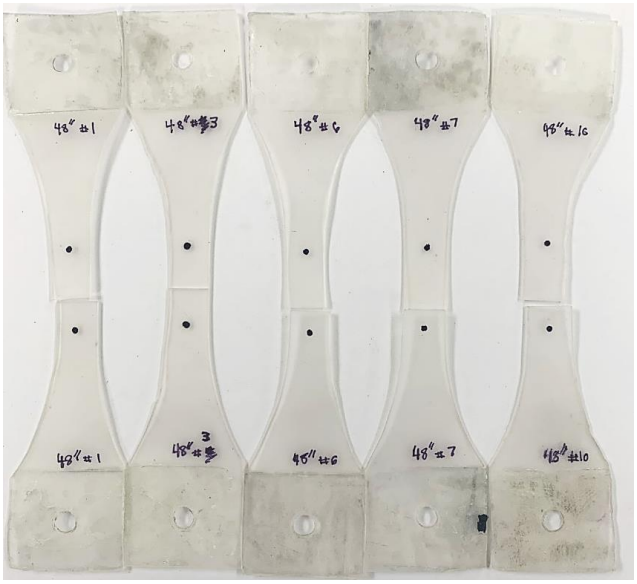

Figure 30: Failed aged PVB drop weight specimens (H = 48 in.).

4.2.2 Summary and Conclusions

In this study, drop weight testing of aged PVB at six different strain rates were performed. The strain-time results were used to verify and calibrate a dynamic model of the drop weight test. The model was proven to accurately predict the strain rate of PVB at any given drop height. The stress-strain relationships for each testing group were analyzed. The results demonstrate that the strain rate greatly effects the initial elastic

response of the interlayer, as well as the total response. As strain rate increases, the initial modulus increases significantly. The stiffness of PVB material contributes to the bending stiffness of laminated glass before glass breakage. Therefore, the strain rate effect on the initial elastic modulus of PVB must be considered to accurately model the behavior of laminated glass systems in blast scenarios. Furthermore, the energy absorption of PVB increases with strain rate. In a dynamic loading scenario, the PVB provides post-cracking energy absorption as it deforms largely. The strain rate effect must be considered in analysis and modeling of post-cracking behavior of laminated glass.

4.2.3 Modifications to Test Procedure

This initial drop weight study was performed on aged PVB left over from previous research efforts, before acquisition of new materials. After completion of this study, several modifications were made to the existing drop weight testing setup and procedure. Several setup modifications have already been discussed previously. Namely, these modifications include the use of a manufactured steel cutting die for accurate specimen geometry and reduction of edge flaws, and the use of a custom template for precise and repeatable marking of the testing gage length onto the specimens. Significant improvements to the data acquisition system and procedure were also made. First, an optical trigger was developed and integrated into the Lab View drop weight program to simultaneously trigger the load cell and the high-speed camera. The synchronization of the subsystem data collection provided many benefits. The shutter-rate of the high-speed camera and the sample rate were both set to 3000 Hz. By triggering both of these systems at the same time, and by the same method, the stress and strain data were therefore

automatically synchronized, which made data analysis much simpler and allowed for easy detection of irregularities even before the data was analyzed. By adjusting the height of the optical trigger with respect to the anvil, the timing of data collection could be optimized. This meant that the relevant data could be isolated. Less bulk data was collected, and the precision of the data could be increased by increasing the sampling rate.

Figure 31: Optical trigger.

Table 3: Comprehensive summary of drop weight testing of aged PVB study.

No.	Specimen	H (in.)	$\dot{\varepsilon}_A$ (s^{-1})	$\dot{\varepsilon}_E$ (s^{-1})	$\sigma_{ps,y}$ (psi)	$\varepsilon_{ps,y}$ (in/in)	σ_f (psi)	ε_f (in/in)	E_{ini} (psi)	E_{sec} (psi)	U (psi·in/in)
1	V-P-060-R-018-1	6	18	13.17	1015	0.143	2932	1.54	7776	1792	2756
2	V-P-060-R-018-2	6	18	16.15	1495	0.202	2878	1.43	8329	1480	2733
3	V-P-060-R-018-3	6	18	12.87	1338	0.214	2942	1.58	6594	1419	3106
4	V-P-060-R-018-4	6	18	12.72	950	0.146	2867	1.50	8243	1744	2766
5	V-P-060-R-018-5	6	18	10.93	1020	0.163	2917	1.51	7207	1985	2639
6	V-P-060-R-029-1	18	31	30.63	1315	0.113	3667	1.29	11819	2183	2903
7	V-P-060-R-029-2	18	31	34.64	1248	0.147	4156	1.54	10690	2437	3631
8	V-P-060-R-029-4	18	31	31.87	913	0.096	4119	1.56	10797	2296	3722
9	V-P-060-R-029-7	18	31	29.34	945	0.049	3121	1.18	11102	2263	2117
10	V-P-060-R-029-8	18	31	29.43	939	0.141	2519	1.17	10694	2068	1763
11	V-P-060-R-033-1	24	35	41.12	1305	0.062	3788	1.36	12133	2005	3235
12	V-P-060-R-033-2	24	35	33.85	1636	0.084	3405	1.24	11315	1984	2500
13	V-P-060-R-033-3	24	35	33.41	1171	0.091	3666	1.39	8288	2155	3080
14	V-P-060-R-033-5	24	35	34.14	888	0.091	4390	1.70	9557	2330	4159
15	V-P-060-R-033-9	24	35	40.14	857	0.062	4430	1.90	16100	2119	4843
16	V-P-060-R-041-1	36	43	39.78	1074	0.089	3933	1.52	14026	2249	3352
17	V-P-060-R-041-3	36	43	44.72	1143	0.118	3653	1.40	16469	2134	3006
18	V-P-060-R-041-5	36	43	38.69	1167	0.132	4243	1.40	12061	2824	3313
19	V-P-060-R-041-7	36	43	45.8	1455	0.190	4171	1.51	13413	2201	3281
20	V-P-060-R-041-8	36	43	37.51	1278	0.117	3980	1.47	11245	2251	3315
21	V-P-060-R-047-1	48	49	44.88	1307	0.161	4696	1.55	9600	2630	3938
22	V-P-060-R-047-3	48	49	52.31	1504	0.174	3895	1.39	15402	2159	2971
23	V-P-060-R-047-6	48	49	47.18	999	0.143	4466	1.74	12042	2389	4340
24	V-P-060-R-047-7	48	49	41.89	869	0.170	3875	1.30	7323	2827	2702
25	V-P-060-R-047-10	48	49	50.86	1478	0.099	4390	1.54	17666	2209	4130
26	V-P-060-R-054-1	64	54	52.30	904	0.103	4702	1.63	8352	2581	4075
27	V-P-060-R-054-6	64	54	50.89	806	0.130	4786	1.73	7003	2544	4275
28	V-P-060-R-054-7	64	54	52.01	622	0.076	3026	1.22	9017	2096	2185

4.3 DROP WEIGHT TESTING OF UNAGED PVB AT VARIOUS TEMPERATURE RANGES AND STRAIN RATES

In this study, six testing groups of PVB of 0.03 in. thickness were performed at two different drop heights and three different temperature ranges. The two drop heights, 19 in. and 43 in., were chosen using the dynamic model described in Section 3.3.5 in order to achieve strain rates of $30s^{-1}$ and $45s^{-1}$. The target temperature ranges of the cold, moderate, and hot temperatures were < 40°F, 55-65°F, and > 80°F, respectively. In this section, the results will be discussed individually for each temperature range, followed by a comprehensive discussion of the temperature and strain rate effects. A summary of the study and conclusions will be stated. Finally, modifications to the testing procedure will be presented.

4.3.1 Test Matrix

The test matrix for this study is given in Table 4.

Table 4: Temperature study test matrix.

Drop Height (in)	# of Specimens	Analytical Strain Rate, $\dot{\varepsilon}_A$ (s^{-1})	Target Temperature Range, °F
19	5	30	<40
19	5	30	55-65
19	5	30	80
43	5	45	<40
43	5	45	55-65
43	5	45	80

4.3.2 Results and Discussion

In this section, the results of the cold, moderate, and elevated temperature ranges will be discussed individually, followed by a comprehensive discussion of temperature and strain rate effects. For these tests, the data analysis is the same as for the aged PVB. In addition, the initial strain in the specimen before impact and the modulus ratio, defined as the ratio of the initial modulus to the secondary modulus, are recorded. The results for every test of this study is summarized in the Appendix.

4.3.2.1 Cold Temperature Range

The cold temperature range was achieved using a small freezer placed nearby the drop weight testing machine. Specimens were left overnight in the freezer. The internal temperature of the freezer was between 0°F and 5°F. Each specimen was removed individually and was immediately tested. The average time out of the freezer before testing was 108 seconds (1 minute and 38 seconds). The ambient temperature was between 55-60°F. The exact temperature of the specimen during impact is not known, but is believed to be below 40°F.

The stress-strain curves for the drop heights of 19 in. and 43 in. are shown in Figure 32 (a) and (b), respectively. A comparison of the average stress-strain curves for each drop height is shown in Figure 33. The average test results are summarized in Table 5.

There are observable differences between the drop heights at the cold temperature range. At the strain rate of 35.2 s^{-1}, the pseudo-yield stress, initial modulus, failure stress, and strain energy are all slightly higher than at the strain rate of 48.9 s^{-1}. The modulus ratio is

also higher for the strain rate of 48.9 s^{-1}. The modulus is used to characterize degree to which the overall behavior is more viscoelastic or elasto-plastic. A curve with a high modulus ratio is more elasto-plastic, whereas a curve with a lower modular ratio is more viscoelastic. It is also observed that the experimental strain rate for both drop heights related well to the predicted strain rates from the analytical model. The percent difference between experimental and analytical strain rate for the drop height of 19 in. is +17.3% and for the drop height of 43 in. is +8.7%.

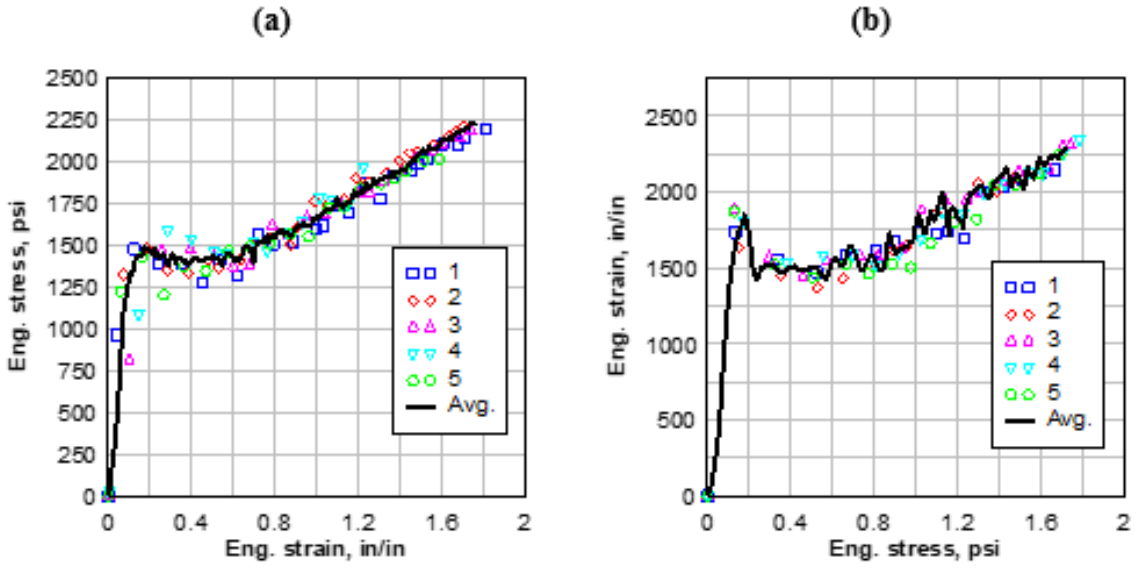

Figure 32: Engineering stress versus engineering strain for cold temperature drop weight tests (a) H=19in. (b) H=43 in.

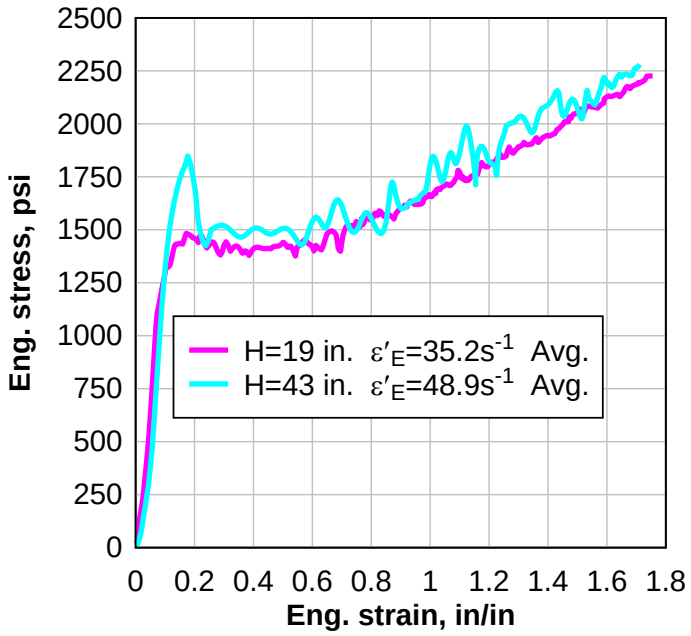

Figure 33: Engineering stress versus engineering strain of cold temperature drop weight tests.

Table 5: Summary of cold temperature drop weight test results.

H (in)	Avg. °F	Avg. $\dot{\varepsilon}_E$ (s^{-1})	ε_{ini} (in/in)	$\sigma_{ps,y}$ (psi)	$\varepsilon_{ps,y}$ (in/in)	σ_f (psi)	ε_f (in/in)	E_{ini} (psi)	E_{sec} (psi)	Modulus Ratio	U (psi·in/in)
19	< 40	35.2	0	1532	0.164	2129	1.633	15126	600	25.2	2594
43	< 40	48.9	0	1965	0.146	2358	1.696	20441	654	31.2	2833

4.3.2.2 Moderate Temperature Range

The moderate temperature range of 55-65°F was achieved by ambient air temperature. The stress-strain curves for the drop heights of 19 in. and 43 in. are shown in Figure 34 (a) and (b), respectively. A comparison of the average stress-strain curves for each drop height is shown in Figure 35. The average test results are summarized in Table 6.

For these tests, the weight of the anvil induced an initial strain in the test specimens before impact of the striker. This effect was observed, and an effort was made to mitigate the issue. The anvil was supported before testing by a wooden post. A string of fishing line was tied around the bottom of one of the rods of the striker, threaded between the gap of the anvil beneath its interior pegs, and tied tightly around the bottom of the other rod of the striker. The idea was that the fishing line would support the weight of the anvil until the test is initiated, after which the tension in the fishing line would be released. However, the fishing line was not stiff enough, and strained under the weight of anvil causing initial strain to be observed in the specimen before impact. At the higher drop height, the fishing line strained more than at the lower drop height, resulting in almost 3 times more initial strain in the 43 in. drop height testing group than in the 19 in. drop height testing group. The amount of initial strain was determined by comparing the distance between the gage length markings at the instant before impact of each specimen to the length between gage length markings of an unstressed specimen. For the colder temperature range, however, the specimens were much stiffer, and this effect was not observed. Initial strain was not observed in the study of aged PVB due to the aged PVB being 1.6 times thicker and much stiffer than the unaged PVB.

The initial strain in the specimens significantly affected the response of the PVB specimens in this testing group. A large increase in strain rate at the 43 in. drop height between the cold and moderate temperature range (+19.7 s^{-1} or +40%) was observed because the initial strain response was not recorded. The initial strain at the higher drop height also resulted in the pseudo-yield strain, initial modulus, and strain energy to be much less than expected. At the same temperature, increase in strain rate should result in

increases in the pseudo-yield stress, initial modulus, failure stress, and strain energy. Also, as strain rate is increased, the behavior of PVB is expected to become more elasto-plastic like, and therefore the modulus ratio should increase; however, this was not observed and the modulus ratio actually decreased.

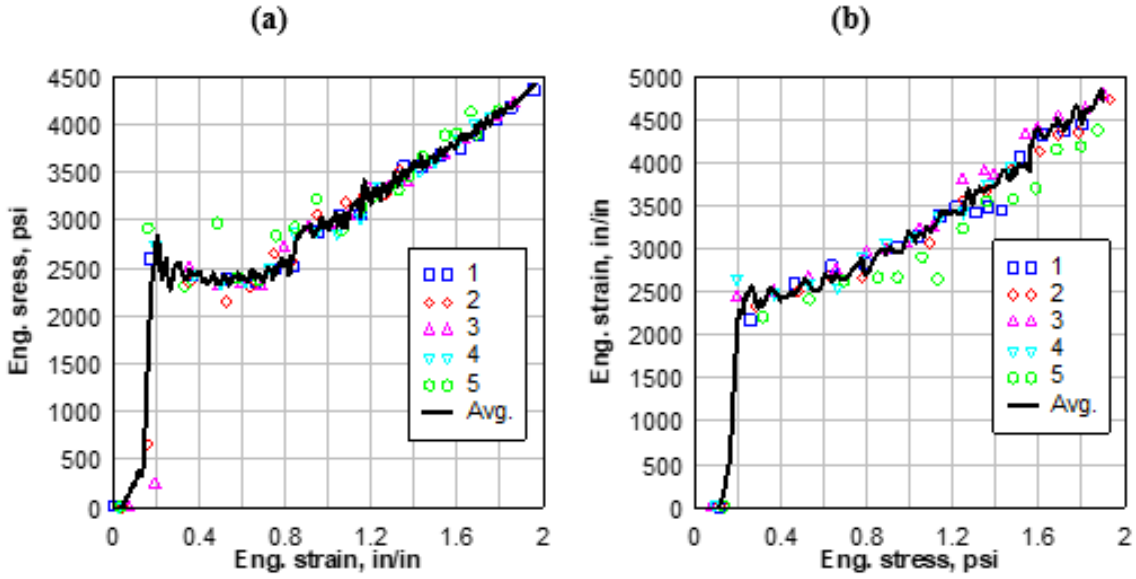

Figure 34: Engineering stress versus engineering strain for moderate temperature drop weight tests (a) H=19in. (b) H = 43 in.

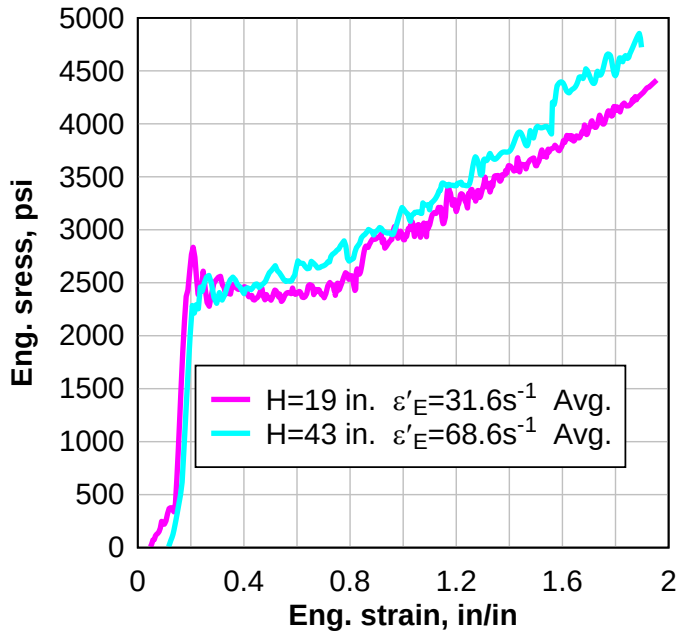

Figure 35: Engineering stress versus engineering strain of moderate temperature drop weight tests.

Table 6: Summary of moderate temperature drop weight test results.

H (in)	Avg. °F	Avg. $\dot{\varepsilon}_{Eav}$ (s^{-1})	ε_{ini} (in/in)	$\sigma_{ps,y}$ (psi)	$\varepsilon_{ps,y}$ (in/in)	σ_f (psi)	ε_f (in/in)	E_{ini} (psi)	E_{sec} (psi)	Modulus Ratio	U (psi·in/in)
19	56	31.6	0.038	3064	0.209	4173	1.793	40113	1308	30.7	5015
43	62	68.6	0.110	2869	0.214	4621	1.851	44578	1511	29.5	5482

4.3.2.3 Elevated Temperature Range

The elevated temperature range of above 80°F was achieved by ambient air temperature. The stress-strain curves for the drop heights of 19 in. and 43 in. are shown in Figure 36 (a) and (b), respectively. A comparison of the average stress-strain curves for each drop height is shown in Figure 37. The average test results are summarized in Table 7.

The average temperature for testing group performed at the drop height of 19 in. is 85.4°F and the average temperature for the testing group performed the drop height of 43 in. is 81.8°F. At elevated temperature range, the PVB becomes less stiff, resulting in increased initial strains under the weight of the anvil. For the testing group performed at the drop height of 19 in., the average initial strain is 0.267 in/in, which is 702% greater than the initial strain of moderate temperature range at the same drop height. The average initial strain for the testing group performed at the drop height of 43 in. is 0.389 in/in (354% increase). The data show that the increase in strain rate at this temperature range has insignificant effects on the response. The failure stress, failure strain, and strain energy to failure are very similar between the two testing groups. At the higher strain rate, the pseudo-yield stress is 1420 psi, which 62% greater than the pseudo-yield stress at the lower strain rate (870 psi). However, the initial modulus decreases by 34% with the increase in strain rate, which is likely due to the higher initial strain of the testing group at the drop height of 43 in. At the same temperature, an increase in strain rate is expected to result in higher pseudo-yield stress and initial modulus (Chen et al. 2018). The modular ratio decreases with increase in strain rate. Therefore, the response becomes more elasto-plastic like as the strain rate is increased.

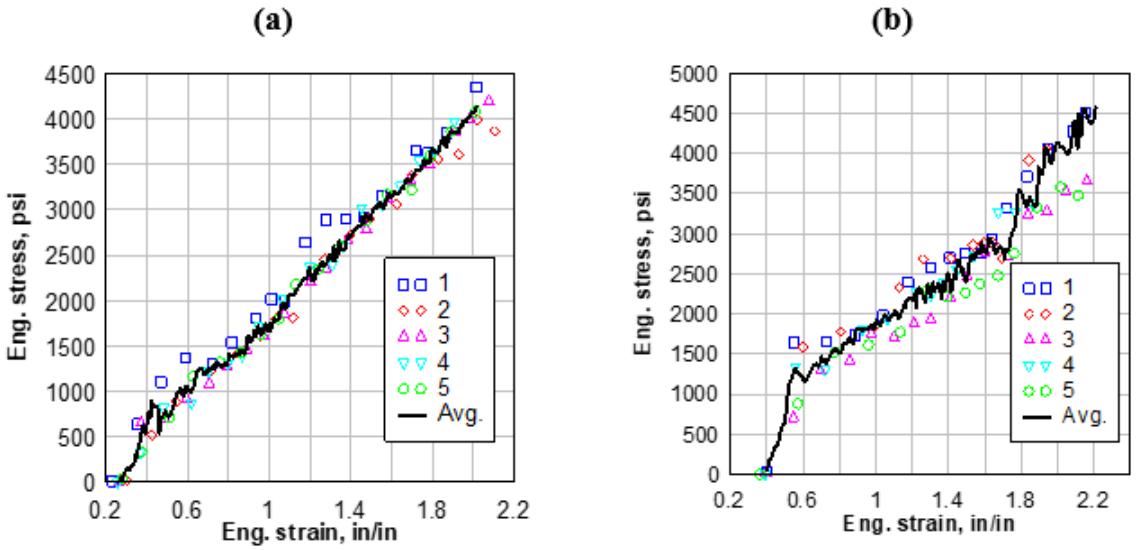

Figure 36: Engineering stress versus engineering strain of moderate temperature drop weight tests.

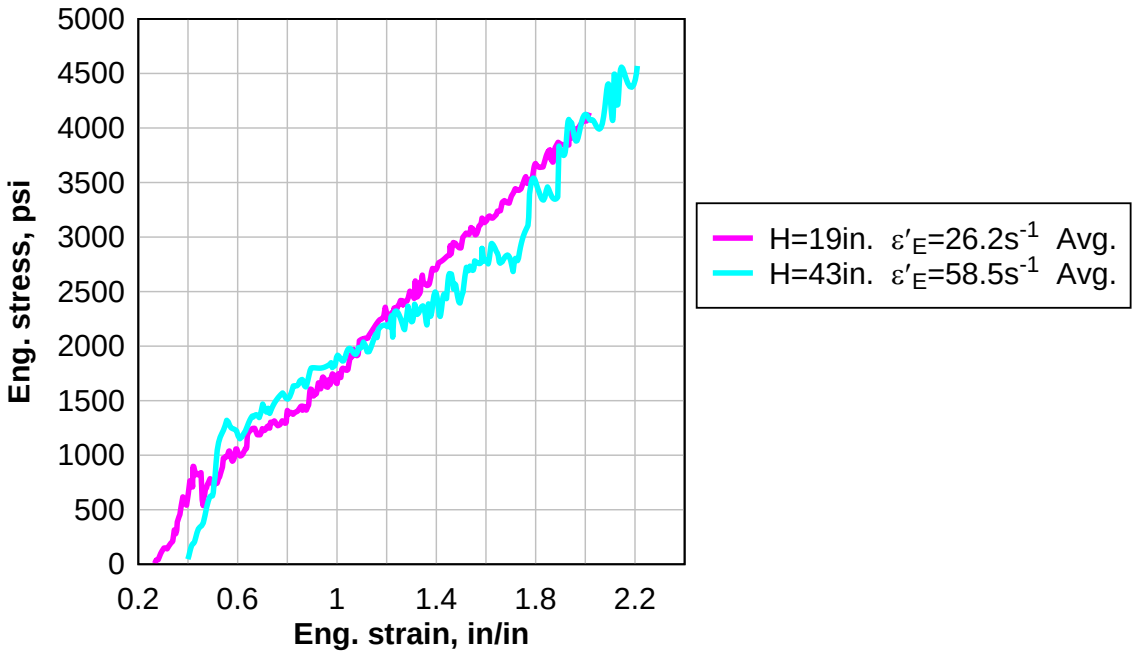

Figure 37: Engineering stress versus engineering strain of hot temperature drop weight tests

Table 7: Summary of elevated temperature drop weight test results.

H (in)	Avg. °F	Avg. $\dot{\varepsilon}_{Eav}$ (s^{-1})	ε_{ini} (in/in)	$\sigma_{ps,y}$ (psi)	$\varepsilon_{ps,y}$ (in/in)	σ_f (psi)	ε_f (in/in)	E_{ini} (psi)	E_{sec} (psi)	Modulus Ratio	U (psi·in/in)
19	85.4	26.2	0.267	879	0.431	4212	2.033	16297	2193	7.4	3914
43	81.8	58.5	0.389	1420	0.597	4054	2.122	10805	1827	5.9	3930

4.3.2.4 Discussion of Temperature and Strain Rate Effects

The average engineering stress versus engineering strain curves for each of the test groups performed in this study are shown in Figure 38. The average results of each testing group are summarized in Table 8.

The behavior of unaged PVB is more brittle at colder temperatures, and is more ductile at elevated temperatures. The failure strain increases as temperature increases. The PVB is significantly weaker at the cold temperature range compared to the moderate temperature range. The average pseudo-yield stresses and failure stresses of the cold temperature range testing groups are roughly 50% less than the moderate range testing groups. This observation contradicts other research on the temperature effects on the mechanical behavior of PVB at high strain rates performed by Chen et al. (2018) and Liao et al. (2019) which found that the pseudo-yield stress and failure stress increase with decreases in temperature. One possible explanation is that the cold temperature testing specimens in this study were exposed to cold temperature for about 24 hours prior to testing. Also, the test specimens were subjected to humidity in the freezer, which was not measured or controlled. At the cold and moderate temperature ranges, the initial elastic response is much more prominent than at elevated temperatures. The pseudo-yield stress and initial

modulus is reduced at the elevated temperature range. This observation relates well to previous research efforts which found that at the same strain rates, as temperature increases the behavior transitions from elasto-plastic-like behavior to viscoelastic behavior (Chen et al. 2018, Zhang et al. 2015). The modulus ratio also characterizes this effect. At cold and moderate temperature ranges, the modulus ratio is about 30, and at elevated temperatures the modulus ratio decreases to about 7. The secondary modulus also increases with increases in temperature.

For each temperature range, the increase in strain rate has minimal effect on the response of unaged PVB. The increases in strain rate resulted in slight increases in strain energy for each temperature range. For cold and moderate temperate groups, the increase in strain rate resulted in increases in pseudo-yield stress, initial modulus, and secondary modulus. The strain rate effect on the elevated temperature range was greatly affected by the large difference in initial strain between the two testing groups.

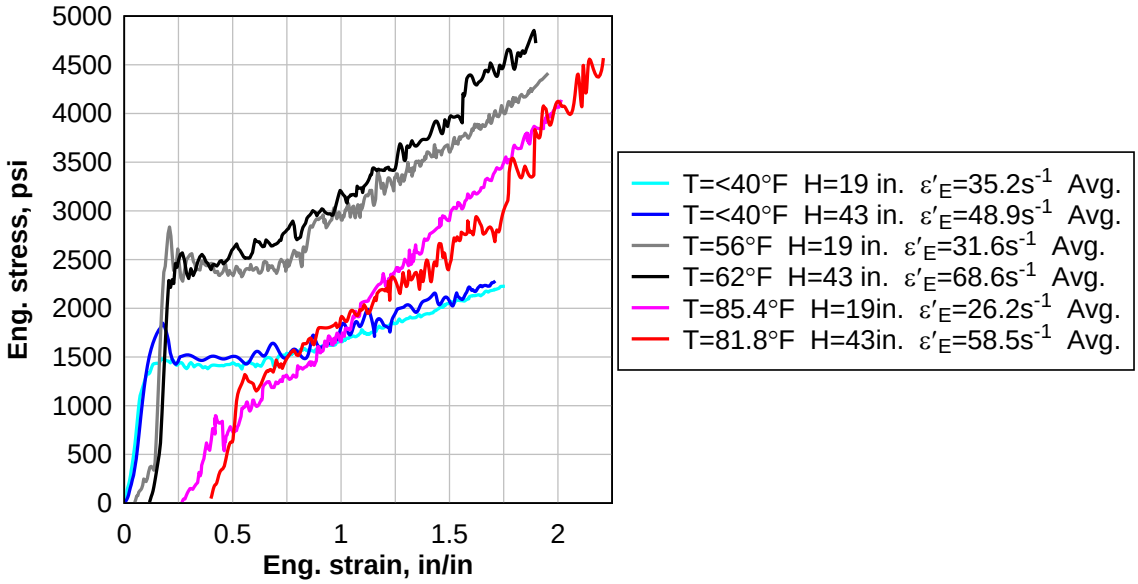

Figure 38: Engineering stress versus engineering strain for unaged PVB specimens tested at two different strain rates and three different temperature ranges.

Table 8: Summary of drop weight testing of unaged PVB under two different strain rates and three different temperature ranges results.

H (in)	Avg. °F	Avg. $\dot{\varepsilon}_E$ (s^{-1})	ε_{ini} (in/in)	$\sigma_{ps,y}$ (psi)	$\varepsilon_{ps,y}$ (in/in)	σ_f (psi)	ε_f (in/in)	E_{ini} (psi)	E_{sec} (psi)	Modulus Ratio	U (psi·in/in)
19	< 40	35.2	0	1532	0.164	2129	1.633	15,126	600	25.2	2594
43	< 40	48.9	0	1965	0.146	2358	1.696	20,441	654	31.2	2833
19	56	31.6	0.038	3064	0.209	4173	1.793	40,113	1308	30.7	5015
43	62	68.6	0.110	2869	0.214	4621	1.851	44,578	1511	29.5	5482
19	85.4	26.2	0.267	879	0.431	4212	2.033	16,297	2193	7.4	3914
43	81.8	58.5	0.389	1420	0.597	4054	2.122	10,805	1827	5.9	3930

4.3.3 Summary and Conclusions

In this study, unaged PVB specimens were tested at three different temperature ranges and two different strain rates. The mechanical behavior of unaged PVB is significantly affected by temperature. At colder temperatures, the response is more elasto-plastic like, and at elevated temperatures, the response is more typical of a viscoelastic material.

Therefore, temperature effects need to be considered to accurately model the post-cracking behavior of laminated glass systems. In the data collected, strain rate effect is minimal; however, due to initial strains in the material at moderate and elevated temperatures which significantly affected the stress-strain responses, the strain rate effect is not able to be accurately characterized. At cold temperatures, the increase in strain rate results in increases in pseudo-yield stress (+28.3%) and initial stiffness (+35.1%).

4.3.4 Modifications to Test Apparatus

In order to minimize the initial strain of the testing material under the rate of the anvil, a lighter anvil was manufactured out of plastic (Figure 39). Also, material cutouts were built into the design to reduce the weight of the anvil. Aluminum plates were screwed to the top to prevent the anvil from being damaged by the impact of the striker. The weight of the plastic anvil is 0.856 pounds, which is less than half the weight of the aluminum anvil (2.02 pounds).

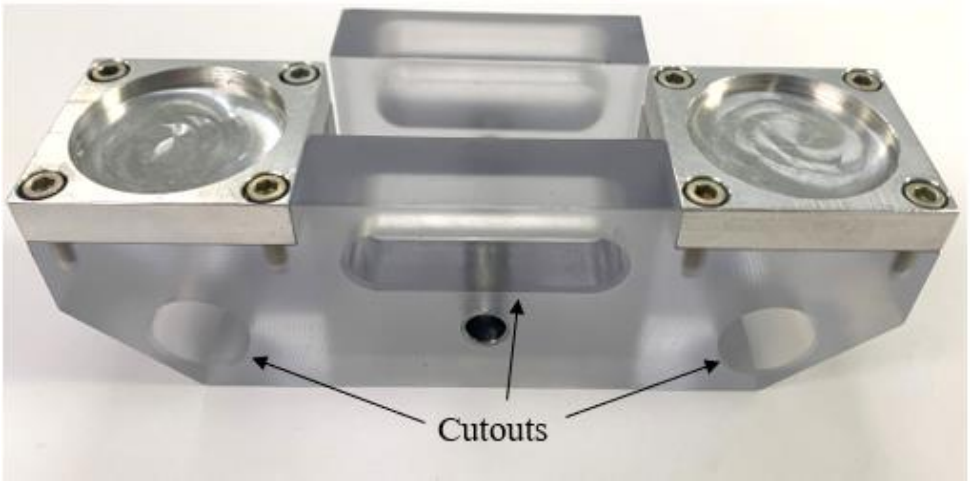

Figure 39: Plastic anvil for clamping drop weight test specimens.

To eliminate any initial strain in the test specimen in future testing, a support frame was made out of aluminum T-slot material (Figure 40). Lengths of weak and brittle material, such as balsa wood, will be placed between frame members to support the anvil before impact. The members of the frame are adjustable to accommodate any changes of the height of the fixed member or specimen geometry. The weak and brittle material will fail immediately upon impact, and therefore will have negligible effect on the loading of the specimen. This support frame will be incorporated into future drop weight testing of interlayer materials.

Figure 40: Anvil support frame.

Table 9: Comprehensive summary of drop weight testing of unaged PVB at various temperature ranges and strain rates study.

No.	Specimen	Temp. (°F)	H (in.)	$\dot{\varepsilon}_A$ (s^{-1})	$\dot{\varepsilon}_E$ (s^{-1})	ε_{ini} (in/in)	$\sigma_{ps,y}$ (psi)	$\varepsilon_{ps,y}$ (in/in)	σ_f (psi)	ε_f (in/in)	E_{ini} (psi)	E_{sec} (psi)	U (psi·in/in)
1	K-P-030-S40F-030-1	< 40	19	30	34.31	0	1444	0.137	2184	1.806	14663	655	2931
2	K-P-030-S40F-030-2	< 40	19	30	31.91	0	1492	0.122	2243	1.769	18658	641	2927
3	K-P-030-S40F-030-3	< 40	19	30	34.78	0	1590	0.211	2199	1.771	9775	587	2865
4	K-P-030-S40F-030-4	< 40	19	30	38.74	0	1625	0.245	1964	1.229	11123	547	1761
5	K-P-030-S40F-030-5	< 40	19	30	36.36	0	1508	0.106	2053	1.590	21411	568	2484
6	K-P-030-60F-030-1	55	19	30	31.68	0.006	2862	0.142	4363	1.955	37059	1337	5748
7	K-P-030-60F-030-2	55	19	30	33.86	0.048	3007	0.224	3836	1.436	52628	1261	3550
8	K-P-030-60F-030-3	56	19	30	31.20	0.072	3194	0.269	4218	1.886	40817	1356	5181
9	K-P-030-60F-030-4	57	19	30	31.17	0.029	2893	0.220	4163	1.793	35181	1328	4988
10	K-P-030-60F-030-5	57	19	30	30.11	0.036	3364	0.189	4284	1.895	34882	1258	5610
11	K-P-030-80F-030-1	81	19	30	26.21	0.23	837	0.309	4349	2.016	22994	2071	4163
12	K-P-030-80F-030-2	85	19	30	25.76	0.299	557	0.406	4120	2.074	8034	2161	4078
13	K-P-030-80F-030-3	86	19	30	28.65	0.265	753	0.44	4197	2.075	20295	2248	3908
14	K-P-030-80F-030-4	87	19	30	24.46	0.257	1215	0.426	4164	1.943	12921	2307	3510
15	K-P-030-80F-030-5	88	19	30	25.91	0.28	1035	0.576	4230	2.055	17242	2176	3909
16	K-P-030-S40F-045-1	< 40	43	45	47.7	0	1907	0.107	2175	1.711	33109	588	2882
17	K-P-030-S40F-045-2	< 40	43	45	50.43	0	1653	0.157	2288	1.536	16105	760	2418
18	K-P-030-S40F-045-3	< 40	43	45	46.83	0	2147	0.154	2658	1.759	21498	702	3031
19	K-P-030-S40F-045-4	< 40	43	45	49.17	0	2127	0.203	2354	1.770	11273	635	2999
20	K-P-030-S40F-045-5	< 40	43	45	50.48	0	1992	0.111	2317	1.703	20221	586	2836
21	K-P-030-60F-045-1	61	43	45	75.52	0.116	2615	0.228	4996	1.880	41849	1529	5698
22	K-P-030-60F-045-2	61	43	45	66.49	0.125	2793	0.256	4734	1.973	24649	1539	5954
23	K-P-030-60F-045-3	62	43	45	67.40	0.076	3226	0.162	4901	1.920	59734	1583	6134
24	K-P-030-60F-045-4	63	43	45	61.83	0.093	2864	0.180	3892	1.560	51954	1414	4304
25	K-P-030-60F-045-5	63	43	45	71.62	0.138	2847	0.243	4582	1.923	44706	1491	5321
26	K-P-030-80F-045-1	83	43	45	55.88	0.400	1726	0.562	4685	2.213	22299	2022	4605
27	K-P-030-80F-045-2	82	43	45	61.81	0.393	1746	0.681	4472	2.083	7243	1827	4160
28	K-P-030-80F-045-3	82	43	45	54.72	0.398	749	0.490	3875	2.212	10620	1741	3894
29	K-P-030-80F-045-4	81	43	45	58.98	0.392	1363	0.541	3383	1.893	9814	1824	3151
30	K-P-030-80F-045-5	81	43	45	61.12	0.362	1514	0.713	3854	2.211	4048	1719	3841

4.4 DROP WEIGHT TESTING OF SG

In this study, five SG coupons of 0.06 in. thickness were tested using the drop weight testing machine at an average strain rate of 50 s^{-1} and average ambient temperature of 63°F. The testing was carried out using the procedure described in Section 3.3. Data analysis was performed using the methods described in Section 4.2.1.1 and Section 4.2.1.3.

4.4.1 Results and Discussion

The average engineering stress versus engineering strain curves for each of the test groups performed in this study are shown in Figure 41. The results for each specimen are summarized in Table 10.

Unlike the PVB specimens, the SG specimens experience noticeable amounts of plastic deformation which can be observed in the failed specimens shown in Figure *42*. However, most of the strain in the specimens is recovered after failure. Therefore, the response of SG at this specific temperature range and strain rate is largely viscoelastic.

The stress-strain response of SG under high strain rate resembles an elasto-plastic like response. Initially there is a very steep rise in stress until pseudo-yielding occurs at a strain of about 0.14, after which the stress decreases until a strain of about 0.45, and then continues to decrease at a very low rate until failure. Therefore, the average pseudo-yielding stress, 7018 psi, is greater than the average failure stress (4942 psi). No initial strain is observed due to the high stiffness of the material. The average strain rate of the

testing group is 50.96 s^{-1}. Compared to the aged PVB testing group with strain rate of 50.1 s^{-1} (H = 48 inches), the response of SG is superior to the response of aged PVB. The results for these two testing groups are summarized in Table 11. The initial modulus, pseudo-yield stress, failure stress, failure strain, and strain energy to failure are all significantly higher for SG than aged PVB. However, the comparison is not a truly direct comparison because the thickness of aged PVB (0.5 inches) is less than the SG (0.6 inches), and tests performed on aged PVB were conducted at a higher temperature range (83.6°F) than the testing temperature of the SG tests (63°F).

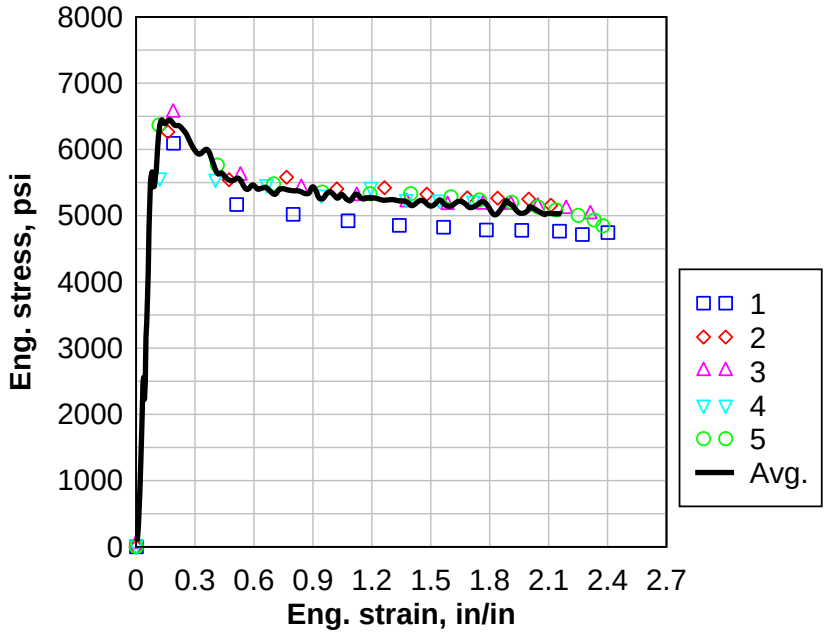

Figure 41: Engineering stress versus engineering strain of SG drop weight test specimens.

Table 10: Summary of drop weight testing of SG results.

Specimen No.	Temp. °F	H (in.)	$\dot{\varepsilon}_E$ (s^{-1})	$\sigma_{ps,y}$ (psi)	$\varepsilon_{ps,y}$ (in/in)	σ_f (psi)	ε_f (in/in)	E_{ini} (psi)	E_{sec} (psi)	U (psi·in/in)
1	64	19	50.98	7444	0.152	4836	2.522	58,677	-284	12,492
2	64	19	47.23	6872	0.117	5180	2.168	64,894	-388	11,727
3	63	19	55.84	6690	0.150	5046	2.346	56,221	-385	12,434
4	62	19	45.94	7516	0.075	4900	1.765	78,835	-473	9,434
5	62	19	54.83	6570	0.199	4746	2.398	65,058	-496	12,777
Average	**63**	**19**	**50.96**	**7018**	**0.139**	**4942**	**2.240**	**64,737**	**-405**	**11,773**

Table 11: Comparison between response of SG and aged PVB at the same strain rate.

Material	Thickness (in.)	Temp. °F	$\dot{\varepsilon}_E$ (s^{-1})	$\sigma_{ps,y}$ (psi)	$\varepsilon_{ps,y}$ (in/in)	σ_f (psi)	ε_f (in/in)	E_{ini} (psi)	E_{sec} (psi)	U (psi·in/in)
SG	0.06	63	50.96	7018	0.139	4942	2.240	64,737	-405	11,773
PVB	0.05	83.6	50.12	1231	0.149	4264	1.504	12,406	2443	3616

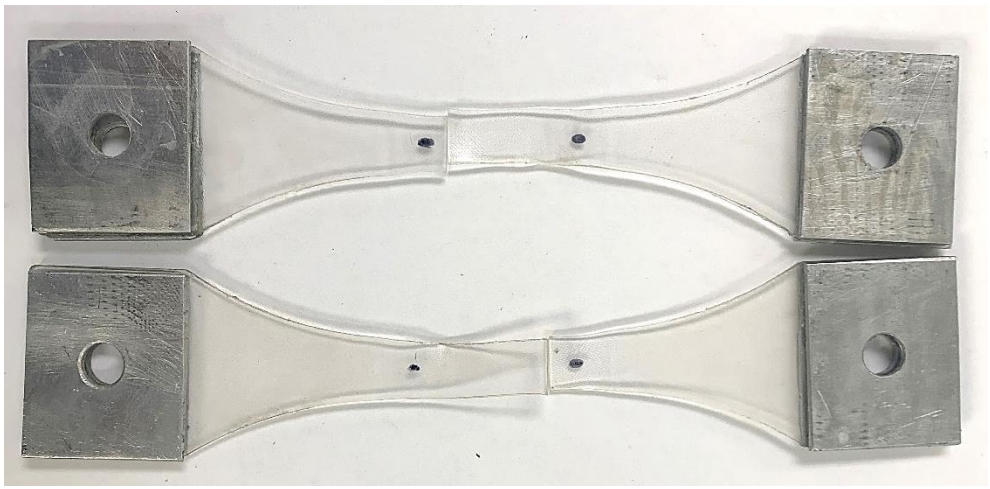

Figure 42: Failed SG drop weight test specimens.

4.4.2 Summary

Engineering stress-strain curves for SG specimens tested at a strain rate of $50s^{-1}$ and moderate temperature range are presented. Although most strain is recovered, the data show that SG behaves essentially like an elasto-plastic material under high strain rate loading. SG has better initial response, stiffer initial modulus and higher pseudo-yield stress, as well as overall response, larger strain to failure and energy absorbed, than aged PVB tested at the same strain rate.

4.5 QUASI-STATIC TESTING OF PVB AND SG

In this study, five unaged PVB coupons of 0.03-inch thickness and five SG coupons of 0.06-inch thickness were tested quasi-statically using the methodology described in Section 3.4. The loading rate was chosen according to ASTM 638-10 (2010) to be 2 inches per minute. All quasi-static tests were performed in a temperature-controlled room and the test temperatures were recorded.

4.5.1 Quasi-static Testing of Unaged PVB

The engineering strain time histories of for unaged PVB are shown in Figure 43. The engineering strain versus time response for each test is linear. The average experimental strain rate, $\dot{\varepsilon}_{Eav}$, for each test is defined as the slope of the line of best fit of the strain time history. For each test, the average experimental strain rate is 0.003 s^{-1}.

The engineering stress-strain responses are shown in Figure 44 and the results are summarized in Table 12. The engineering stress-strain response of unaged PVB is highly nonlinear. Under quasi-static loading, the polymer behaves in a highly nonlinear, hyperelastic manner. As the material strains, it stiffens continuously until failure occurs at very large strain; however, no plastic deformation occurs. All of the strain is recovered after failure, as shown in the failed specimen (Figure 45). The average failure stress is 3651 psi and the average failure strain is 2.691 in/in. The average strain energy to failure is 3387 psi·(in/in).

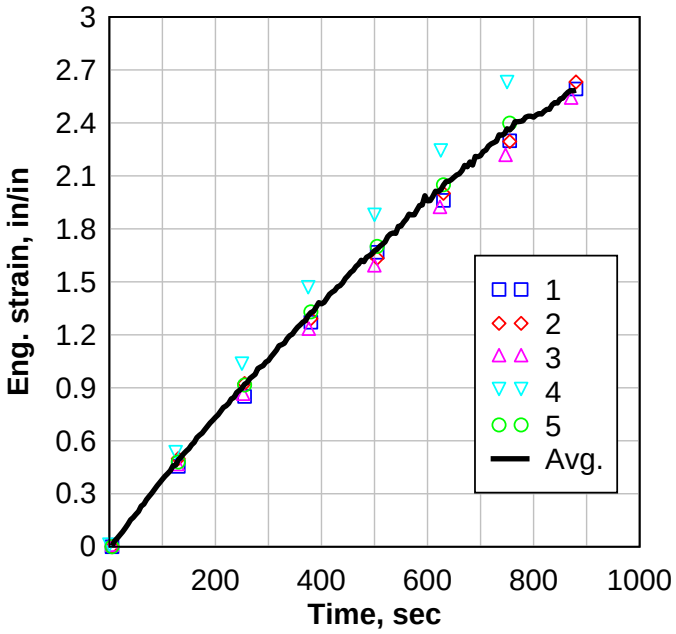

Figure 43: Engineering strain time histories of unaged PVB specimens under quasi-static loading.

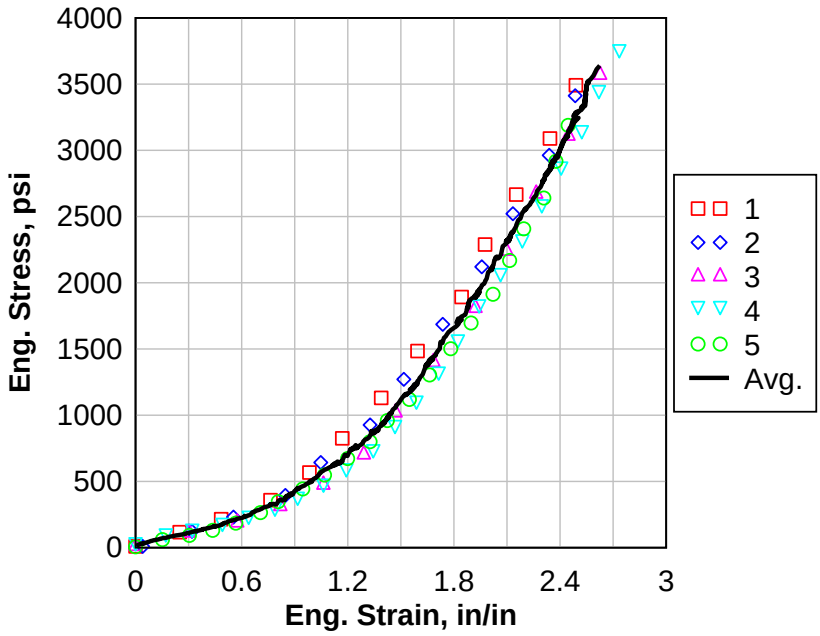

Figure 44: Engineering stress versus engineering strain of unaged PVB specimens under quasi-static loading.

Table 12: Summary of unaged PVB quasi-static testing results.

No.	Temp. °F	$\dot{\varepsilon}_{Eav}$ (s^{-1})	σ_f (psi)	ε_f (in/in)	U (psi·in/in)
1	69	0.003	3741	2.626	3511
2	69	0.003	3736	2.665	3502
3	69	0.003	3821	2.782	3598
4	69	0.003	3890	2.831	3596
5	69	0.003	3255	2.550	2730
Average	**69**	**0.003**	**3689**	**2.691**	**3387**

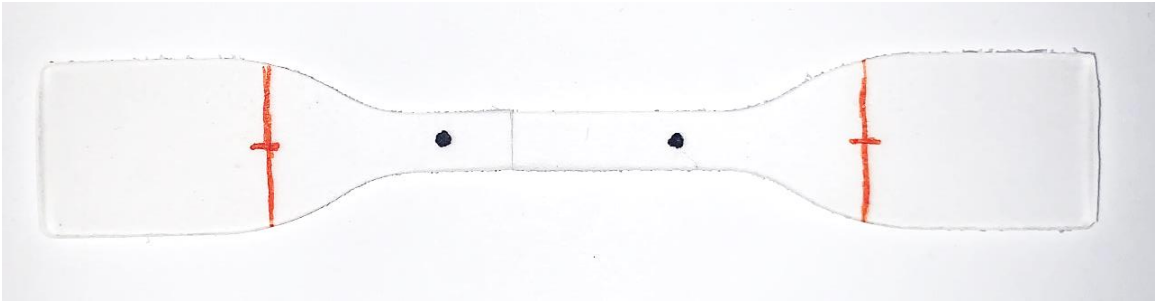

Figure 45: Failed unaged PVB quasi-static test specimen.

4.5.2 Quasi-static Testing of SG

The engineering strain time histories of for unaged PVB are shown in Figure 46. The engineering strain versus time response is linear until a strain of about 1.35, then the decreases steadily with time until a strain of about 1.9, after which the slope of the becomes linear again until failure. The segment of decreasing strain rate corresponds to strain hardening in the stress strain curve (Figure 47). The average experimental strain rate, $\dot{\varepsilon}_{Eav}$, for each test is about $0.0015s^{-1}$.

Under quasi-static loading, the stress-strain response is elasto-plastic like, with strain hardening occurring at large strains. The initial response is very stiff until pseudo-yielding. The average initial modulus is 53,452 psi and the average pseudo-yield stress is 4388 psi. The stress decreases to about 3500 psi directly after pseudo-yielding, and stays constant until the strain hardening region. After strain hardening, the stress increases linearly until failure. The average failure stress is 6520 psi and the average failure strain is 2.861 in/in. The strain energy to failure is 11,916 psi·in/in. Large amounts of plastic deformation are observable in the failed specimens shown in Figure 48.

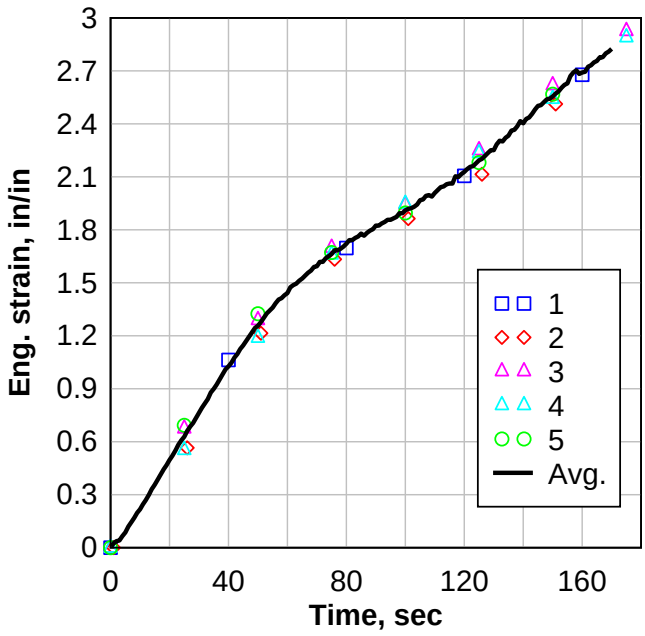

Figure 46: Engineering strain time histories of SG specimens under quasi-static loading.

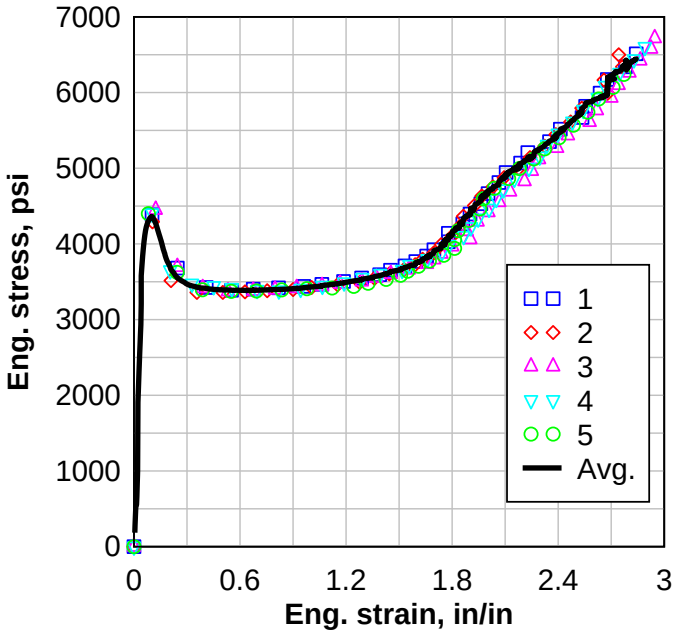

Figure 47: Engineering stress versus engineering strain of SG specimens under quasi-static loading.

Table 13: Summary of SG quasi-static testing results.

No.	Temp. °F	$\dot{\varepsilon}_E$ (s^{-1})	$\sigma_{ps,y}$ (psi)	$\varepsilon_{ps,y}$ (in/in)	σ_f (psi)	ε_f (in/in)	E_{ini} (psi)	E_{sec} (psi)	U (psi·in/in)
1	68	0.015	4389	0.100	6516	2.801	49,302	1242	11,676
2	68	0.015	4296	0.096	6390	2.764	49,679	1126	11,371
3	68	0.016	4453	0.123	6726	2.946	47,853	1191	12,294
4	68	0.016	4403	0.100	6669	2.980	54,014	1146	12,674
5	68	0.015	4400	0.082	6300	2.813	66,410	1098	11,565
Average	**68**	**0.0154**	**4388**	**0.100**	**6520**	**2.861**	**53,452**	**1161**	**11916**

Figure 48: Failed SG quasi-static test specimens.

4.5.3 Quasi-static Testing Comparison: PVB and SG

The behavior of PVB and SG under quasi-static contrasts starkly (Figure 49). PVB behaves as a highly nonlinear hyperelastic material, whereas SG behaves as an elasto-plastic material that experiences strain hardening at very large strains. The failure stress of SG (6520 psi) is roughly two times greater than that of PVB (3689 psi). The failure strains of the materials are about equal. The strain energy to failure of SG (11,916 psi·in/in) more than three times greater than PVB (3387psi·in/in).

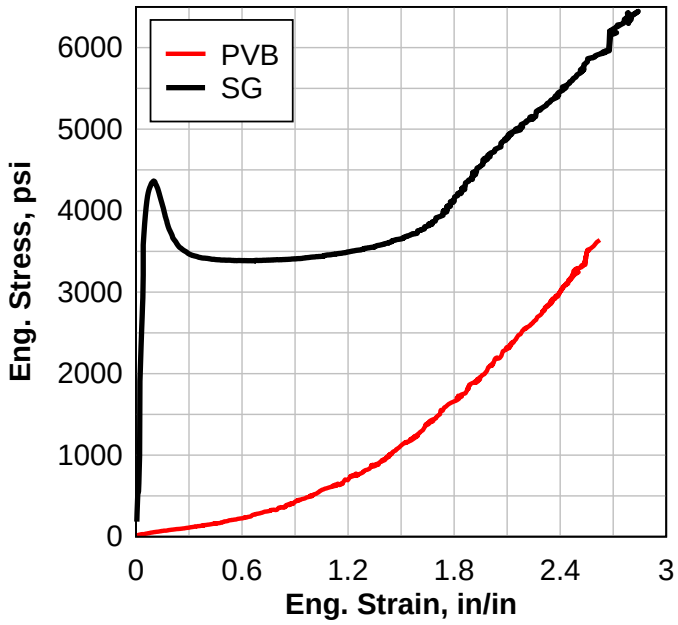

Figure 49: Engineering stress versus engineering strain for PVB and SG under quasi-static loading.

Table 14: Summary of unaged PVB and SG quasi-static testing results.

Material	Temp. °F	$\dot{\varepsilon}_{Eav}$ (s^{-1})	σ_f (psi)	ε_f (in/in)	U (psi·in/in)
PVB	69	0.003	3689	2.691	3387
SG	68	0.015	6520	2.861	11916

4.5.4 Quasi-Static Versus Dynamic Responses: PVB and SG

The dynamic and quasi-static engineering stress-strain response of PVB is shown in Figure 50. For this comparison, the dynamic response curve is that of the aged PVB tested using the drop weight machine with strain rate of $43s^{-1}$. The dynamic response of PVB is bilinear, consisting of an initial linear elastic region until pseudo-yielding followed by a viscoelastic linear portion until failure. The quasi-static response of PVB is

hyperelastic. The material stiffens continuously until failure. The failure stress of the dynamic response (3996 psi) is slightly greater than the failure stress of the static response (3689 psi); however, the failure strain of the quasi-static response (2.691 in/in) is much larger than the dynamic response (1.46 in/in). The strain energy to failure of the dynamic response increases with strain rate, as discussed in Section 4.2. For this particular dynamic response, the strain energy to failure (3253 psi·in/in) is about equal to the strain energy to failure of the static response (3387 psi·in/in).

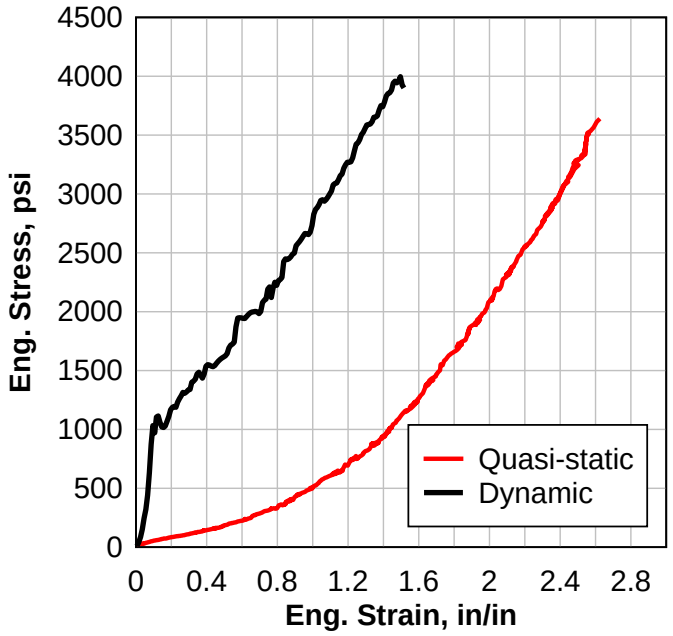

Figure 50: Dynamic and quasi-static engineering stress-strain response of PVB.

Table 15: Summary of dynamic and quasi-static response of PVB.

Response	Temp. °F	$\dot{\varepsilon}_{Eav}$ (s^{-1})	σ_f (psi)	ε_f (in/in)	U (psi·in/in)
Dynamic	83.6	42.4	3996	1.46	3253
Quasi-static	69	0.003	3689	2.691	3387

The dynamic and static engineering stress-strain response of SG is shown in Figure 51. Both the dynamic and static response of SG can is elasto-plastic like; however, after yielding, the static response of SG has a strain hardening region at very large strains while the dynamic response does not. The increase in strain rate causes significant increases in initial modulus (+21.1%), pseudo-yield stress (60.0%), and pseudo-yield strain (+39.0%). Due to the strain hardening effect, the quasi-static response has far larger failure stress (+31.9%) and failure strain (+27.7%) than the dynamic response. This resulted in the strain energy to failure of the static response (11,916 psi·in/in) to be slightly greater than that of the dynamic response (11,772 psi·in/in) despite the strain rate effects on the initial linear elastic portion of the dynamic response.

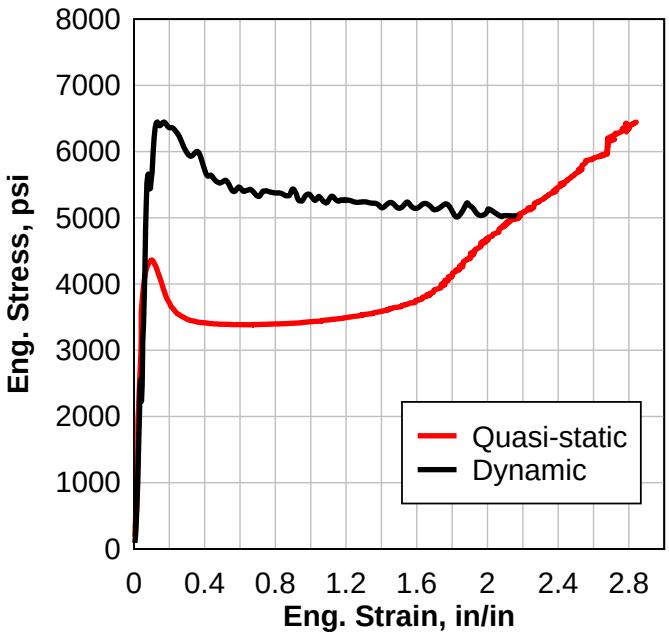

Figure 51: Dynamic and quasi-static engineering stress-strain response of SG.

Table 16: Summary of dynamic and quasi-static response of SG.

Response	Temp. °F	$\dot{\varepsilon}_{Eav}$ (s^{-1})	$\sigma_{ps,y}$ (psi)	$\varepsilon_{ps,y}$ (in/in)	σ_f (psi)	ε_f (in/in)	E_{ini} (psi)	E_{sec} (psi)	U (psi·in/in)
Dynamic	63	50.96	7018	0.139	4942	2.240	64,737	-405	11,772
Quasi-static	68	0.015	4388	0.100	6520	2.861	53,452	1161	11,916

4.5.4 Summary

In this study, five coupons of SG and unaged PVB were tested quasi-statically. PVB behaves as a hyperelastic material at low strain rate, continuously stiffening until failure. All the strain is recovered after failure. SG behaves as an elasto-plastic like material initially and undergoes strain hardening at large strains. Significant plastic deformation is observable in the failed specimens of SG. Comparisons between the dynamic and quasi-static responses show that the strain rate has different and significant effects on the mechanical behavior of PVB and SG.

CHAPTER 5 - CONCLUSIONS, RECOMMENDATIONS, AND FUTURE WORK

5.1 CONCLUSIONS

Dynamic and quasi-static testing were performed to experimentally evaluate the strain rate and temperature effects on the mechanical response of two types of interlayer materials, PVB and SG, commonly used in laminated glass glazing systems. A dynamic model of an existing drop weight testing method was constructed to predict the experimental strain rate at any drop height. The dynamic model was verified and calibrated with experimental results. The existing drop weight testing procedure was improved by the incorporation of an optical trigger to simultaneously trigger the Lab View drop weight program and the high-speed camera. The synchronization of load and displacement data collection streamlined data collection and analysis, allowing for increased sampling rates and real-time detection of data irregularities. The following conclusions were observed from the studies presented in this thesis:

- The dynamic response of PVB is dependent on the strain rate. The strain rate affects the initial linear elastic region before pseudo-yielding more than the viscoelastic response after pseudo-yielding. In general, as strain rate increases, initial modulus and pseudo-yield strength increase, resulting in raised failure stress and strain energy to failure.

- Increases in strain rate result in increases in dynamic strength of PVB; however, the strain rate does not significantly impact the failure strain of the dynamic response of PVB.
- Temperature has more pronounced effects dynamic response of PVB than strain rate.
- Failure strain of the dynamic response of PVB is highly dependent on temperature. As temperature increases, the failure strain of PVB increases.
- At colder temperatures, the initial elastic portion of the dynamic response of PVB before pseudo-yielding is more prominent, and the at elevated temperatures the secondary viscoelastic response is more prominent. The ratio between the initial modulus and secondary modulus decreases as temperature increases.
- The initial elastic response and overall dynamic response of SG is superior to the dynamic response of PVB at the same rate. The initial modulus and pseudo-yield stress of SG are roughly five times greater than PVB. The failure stress of SG is about 15% higher and the failure strain is about 50% higher than PVB. The total strain energy to failure is roughly three times greater for SG compared to PVB.
- The overall shape of the dynamic response is different for PVB and SG. The dynamic response of SG resembles an elasto-plastic response with an extremely steep increase in stress before pseudo-yielding, after which the stress decreases at a very low rate until failure. The dynamic response of PVB is bilinear, consisting of a relatively steep linear region before pseudo-yielding and a flatter linear increase in stress until failure after pseudo-yielding. The ratio between the initial

modulus and secondary modulus ranges between about 5 and 30 for PVB depending on temperature and strain rate.

- The quasi-static response is distinctly different for PVB and SG. Under quasi-static loading, PVB behaves as a highly nonlinear, hyperelastic material which strains elastically even at large strains. SG behaves as an elasto-plastic material and experiences strain hardening and plastic deformation at large strains.
- The initial modulus and pseudo-yield strength of SG are increased under dynamic loading. However, the failure stress and failure strain of the static response are significantly higher than that of the dynamic response due to the strain hardening effect. These combined effects resulted in the strain energies to failure to be about equal for the dynamic and static responses of SG.

5.2 RECOMMENDATIONS

The results of this research thesis can be used for to improve the analytical and numerical modeling of laminated glazing systems under high strain rate loading scenarios, such as blast. The stress-strain response of PVB and SG can be used to develop material models for laminated glass interlayers which are used as input to such analytical and numerical models. Additionally, the failure strengths ratios between dynamic and static responses of PVB and SG can be used to provide recommendations for dynamic increase factors (DIF) for single degree of freedom (SDOF) solutions used by blast design engineers.

The main limitations of this research are the initial strain in the test specimens due to the weight of the anvil and the inability to control temperature and humidity of the testing

conditions. The problem of the initial straining of test specimens due to the weight of the anvil needs to be mitigated, preferably eliminated, in order to accurately study interlayers of 0.03-inch thickness, very flexible interlayer materials such as ethyl vinyl acetate (EVA), and drop weight tests performed at elevated temperatures. Two solutions to this problem, the plastic anvil and the anvil support frame, should be investigated. The temperature should be controlled and monitored through the use of a temperature enclosure around the drop weight machine in order to accurately study the temperature effects on the dynamic response of interlayer materials.

5.3 FUTURE RESEARCH

For future drop weight testing, the modifications describe in Section 4.3.4 will be implemented. The plastic anvil as well as the anvil frame will be tested. These modifications will eliminate the problem of initial strain in the specimens before impact. Also, temperature-controlled drop weight testing will be performed using the temperature enclosure shown in (Figure 52). The temperature enclosure is made of 2-inch-thick insulating foam and has a window in the front so that the strain data can be collected from the high-speed camera outside of the chamber. Using the temperature control air conditioner and ventilator shown in Figure 53 (a) and (b), respectively, temperature tests will be performed at a range of temperatures between 0°F and 120°C. The temperature and humidity will be precisely controlled and measure, which will allow for more accurate characterization of the temperature effects on the dynamic response of laminated glass interlayer polymers.

Figure 52: Temperature enclosure for drop weight testing machine.

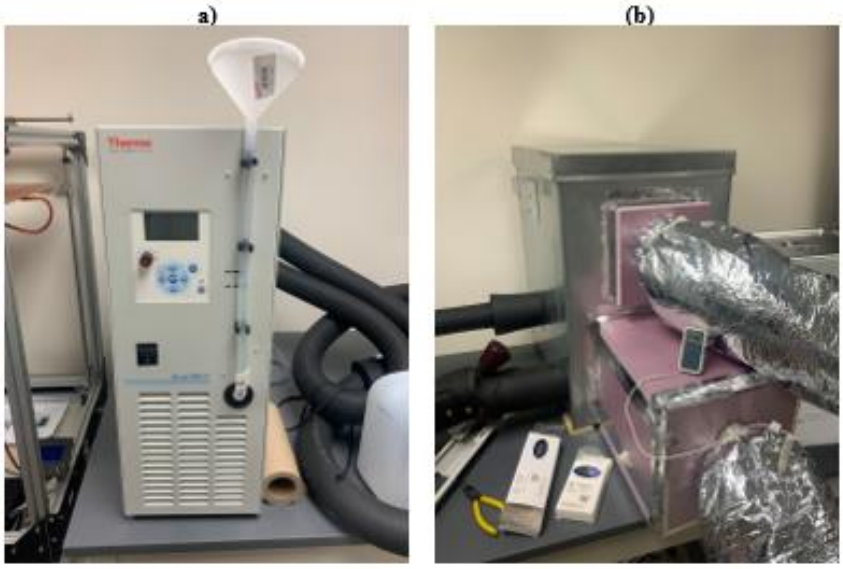

Figure 53: Temperature control: (a) air conditioner (b) air ventilator.

REFERENCES

ANSYS, I. (2017). *ANSYS Release 18.1 Documentation*.

ASTM International. *D638-10 Standard Test Method for Tensile Properties of Plastics*. West Conshohocken, PA, 2010. DOI: https://doi.org/10.1520/D0638-10.

ASTM International. *E1300-16 Standard Practice for Determining Load Resistance of Glass in Buildings*. West Conshohocken, PA, 2016. DOI: https://doi.org/10.1520/E1300-16.

ASTM International. *F2248-19 Standard Practice for Specifying an Equivalent 3-Second Duration Design Loading for Blast Resistant Glazing Fabricated with Laminated Glass*. West Conshohocken, PA, 2019. DOI: https://doi.org/10.1520/F2248-19.

Aymerich, F., Marcialis P., Meili, S., and Priolo, P. (1996). Instrumented drop-weight machine for low-velocity impact testing. Proceedings of the 1996 4th International Conference on Structures Under Shock and Impact, SUSI 96, July 1, 1996 - July 1, 1996, Udine, Italy, Computational Mechanics Inc. URL: https://www.witpress.com/Secure/elibrary/papers/SUSI96/SUSI96022FU.pdf.

Behr, R.A., Minor, J. E., Linden, M. P., and Vallabhan, C. V. G. (1985). Laminated glass units under uniform lateral pressure. *Journal of Structural Engineering*, ASCE, 111(5): 1037-1050. DOI: https://doi.org/10.1061/(ASCE)0733-9445(1985)111:5(1037).

Behr, R.A. and Linden, M. P. (1986). Load duration and interlayer thickness effects on laminated glass. *Journal of Structural Engineering*. ASCE, 112(6), 1141–1153. DOI: https://doi.org/10.1061/(ASCE)0733-9445(1986)112:6(1441).

Bennison, S., Sloan, J. G., Kistunas, D. F., Buehler, P. J., Amos, T., and Smith, C. A. (2005). Laminated Glass for Blast Mitigation: Role of Interlayer Properties. *Glass Processing Days*, 9; 494-496. URL: http://glasslaminatingsolutions.kuraray.com/fileadmin/user_upload/technical_information/downloads/whitepapers/Laminated_glass_for_blast_mitigation_role_of_interlayer_properties.pdf.

Chen, S., Chen, X., and Wu, X. (2018). The mechanical behaviour of polyvinyl butyral at intermediate strain rates and different temperatures. *Construction and Building Materials*, *182*, 66–79. DOI: https://doi.org/10.1016/j.conbuildmat.2018.06.080.

Chen, S., Lu, Y., Zhang, Y., and Shao, X. (2020). Experimental and analytical study on uniaxial tensile property of ionomer interlayer at different temperatures and strain rates. *Construction and Building Materials*, *262*, 120058. DOI: https://doi.org/10.1016/j.conbuildmat.2020.120058.

Chopra, A.K. (2012). *Dynamics of Structures 4th Edition*. *Journal of Chemical Information and Modeling*.

Ding, C., Ngo, T., Mendis, P., Lumantarna, R., and Zobec, M. (2016). Dynamic response of double skin façades under blast loads. *Engineering Structures*, 123, 155–165. DOI: https://doi.org/10.1016/j.engstruct.2016.05.051.

Duser A.V., Jagota A., and Bennison S.J. (1999). Analysis of glass/polyvinyl butyral laminates subjected to uniform pressure. *Journal of Engineering Mechanics*, 125(4):435e42. DOI: https://doi.org/10.1061/(ASCE)0733-9399(1999)125:4(435).

Hooper, J.A. (1973). On the Bending of Architectural Laminated Glass. *International Journal of Mechanical Science (*Great Britain), 15, 309–323. Date accessed: November 20, 2020.

Kleiner, M., Tekkaya, A. E., Demir, O. K., Risch, D., and Psyk, V. (2009). A drop-weight high-speed tensile testing instrument. *Production Engineering*, *3*(2), 175–180. DOI: https://doi.org/10.1007/s11740-009-0154-4.

Lafta, M. (2012). "Experimental evaluation of laminated glass interlayer under high strain rates." M.Sc. dissertation, Univ. of Missouri, Columbia, MO.

Larcher, M., Solomos, G., Casadei, F., and Gebbeken, N. (2012). Experimental and numerical investigations of laminated glass subjected to blast loading. *International Journal of Impact Engineering*, *39*(1), 42–50. DOI: https://doi.org/10.1016/j.ijimpeng.2011.09.006.

Liao, Z., Yao, X., Zhang, L., Hossain, M., Wang, J., and Zang, S. (2019). Temperature and strain rate dependent large tensile deformation and tensile failure behavior of transparent polyurethane at intermediate strain rates. *International Journal of Impact Engineering*, *129*(March), 152–167. DOI: https://doi.org/10.1016/j.ijimpeng.2019.03.005.

Linden, M. P., Minor, J. E., and Vallabhan, C. V. G. (1984). Evaluation of laterally loaded glass units by theory and experiment, supplemental report No. I. *NTIS Accession No. PB85-1 I1532*, Glass Res. and Testing Lab., Texas Tech Univ., Lubbock, Tex. Date accessed: November 24, 2020.

Martín, M., Centelles, X., Solé, A., Barreneche, C., Fernández, A. I., and Cabeza, L. F. (2020). Polymeric interlayer materials for laminated glass: A review. *Construction and Building Materials*, *230*. DOI: https://doi.org/10.1016/j.conbuildmat.2019.116897.

Minor, J. E. and Reznik, P. L. (1990). Failure strengths of laminated glass. *Journal of Structural Engineering*, ASCE, 116(4), 1030-1039. DOI: https://doi.org/10.1061/(ASCE)0733-9445(1990)116:4(1030).

Morrison, C. (2007). "The resistance of laminated glass to blast pressure loading and the coefficients for single degree of freedom analysis of laminated glass." Ph.D. dissertation. Cranfield Univ., Bedford, U.K. URI: http://dspace.lib.cranfield.ac.uk/handle/1826/4651.

National Consortium for the Study of Terrorism and Responses to Terrorism (START), University of Maryland. (2019). The Global Terrorism Database (GTD) [Data file]. Retrieved from https://www.start.umd.edu/gtd.

Nawar, M. (2016). "Numerical modeling and experimental evaluation of laminated glazing systems and material under blast loading." University of Missouri.

Nemat-Nasser, S. (2000). Introduction to High Strain Rate Testing. *ASM Handbook*, 8, 427–428. DOI: https://doi.org/10.31399/asm.hb.v08.a0003293.

Norville, H. S., King, K. W., and Swofford, J. L. (1998). ''Behavior and strength of laminated glass.'' *Journal of Engineering Mechanics*, ASCE, 124(1), 46–53. DOI: https://doi.org/10.1061/(ASCE)0733-9399(1998)124:1(46).

Norville, H. S., Harvill, N., Conrath, E. J., Shariat, S., and Mallonee, S. (1999). Glass-related injuries in Oklahoma City bombing. *Journal of Performance of Constructed Facilities*, 13(2), 50-56. DOI: https://doi.org/10.1061/(ASCE)0887-3828(1999)13:2(50).

Roff , W.J. and Scott, J.R. (1971). Fibres, Films, Plastics and Rubbers—A Handbook of Common Polymer. Butterworth-Heinemann. URL: https://books.google.com/books?hl=en&lr=&id=FPIkBQAAQBAJ&oi=fnd&pg=PP1&ots=lu2cvRyJyM&sig=5mhYa_RC8OCZMnuEjIXP19-h-mk#v=onepage&q&f=false.

Teotia, M. and Soni, R. K. (2014). Polymer Interlayers for Glass Lamination - A Review. *International Journal of Science and Research*, *3*(8), 1264–1270. Obtained from: www.ijsr.net.

Unified Facilities Criteria (UFC). (2014). Structures to resist the effects of accidental explosions. U.S. Department of Defense. Washington, D.C. Obtained from: https://www.wbdg.org/ffc/dod/unified-facilities-criteria-ufc/ufc-3-340-02.

Unified Facilities Criteria (UFC). (2020). DoD Minimum Antiterrorism Standards for Buildings. U.S. Department of Defense. Washington, D.C. Obtained from: https://www.wbdg.org/ffc/dod/unified-facilities-criteria-ufc/ufc-4-010-01.

Vallabhan, C. V. G., Das, Y. C., Magdi, M., Asik, M., and Bailey, J. R. (1993). Analysis of laminated glass units. *Journal of Structural Engineering*, 119(5), 1572–1585. DOI: https://doi.org/10.1061/(ASCE)0733-9445(1993)119:5(1572).

Vallabhan, C. V. G., Minor, J. E., and Nagalla, S. (1987). ‘‘Stresses in layered glass units and monolithic glass plates.’’ J. Struct. Engrg., ASCE, 113(1), 36–43. DOI: https://doi.org/10.1061/(ASCE)0733-9445(1987)113:1(36)

Vallabhan, C. V. G. (1983). Iterative Analysis of Nonlinear Glass Plates. *Journal of Structural Engineering*, *109*(2), 489–502. DOI: https://doi.org/10.1061/(asce)0733-9445(1983)109:2(489)

Wei, J., Shetty, M. S., and Dharani, L. R. (2006). Stress characteristics of a laminated architectural glazing subjected to blast loading. *Computers and Structures*, *84*(10–11), 699–707. DOI: https://doi.org/10.1016/j.compstruc.2005.11.007.

Weller, B. and Kothe, M. (2011). Ageing Behaviour of Polymeric Interlayer Materials and Laminates. *Glass Performance Days, June 2011*, 240–243. URL: https://www.researchgate.net/publication/278004339_Ageing_Behaviour_of_Polymeric_Interlayer_Materials_and_Laminates/link/57d7f20508ae0c0081edd502/download.

Zhang, X. and Bedon, C. (2017). Vulnerability and Protection of Glass Windows and Facades under Blast: Experiments, Methods and Current Trends. *International Journal of Structural Glass and Advanced Materials Research*, *1*(2), 10–23. DOI: https://doi.org/10.3844/sgamrsp.2017.10.23